Single-cell transcriptomic and TCR analysis of human Cytomegalovirus (hCMV)-specific memory T cells reveals effector and pre-effectors of CD8$^+$- and CD4$^+$-cytotoxic T cells

Running title: Single-cell RNA-Seq analysis of hCMV-specific T cells

Raunak Kar[1], Somdeb Chattopadhyay[1], Anjali Sharma[2,#], Kirti Sharma[1,#], Shreya Sinha[1], Gopalakrishnan Aneeshkumar Arimbasseri[1,*], Veena S. Patil[1,*,$]

[1]National Institute of Immunology, Aruna Asaf Ali Marg, New Delhi

[2]Vardhman Mahavir Medical College and Safdarjung Hospital, New Delhi.

[#] Equal contribution

[*]Correspondence can be addressed to GAA (aneesh@nii.ac.in) or VSP (veena@nii.ac.in)

[$]Lead contact

Key Words: hCMV, antigen-specific T cells, CD4-CTLs, CD8-CTLs, T_{REGs}, single-cell RNA-Seq, single-cell TCR-Seq, TCR

Abstract

Background

Latent human Cytomegalovirus (hCMV) infection can pose a serious threat of reactivation and disease occurrence in immune-compromised individuals. Though, T cells are at the core of the protective immune response to hCMV infection, a detailed characterization of different T cell subsets involved in hCMV immunity is lacking.

Results

Here, in an unbiased manner, we characterized over 8000 hCMV-reactive peripheral memory T cells isolated from seropositive human donors, at a single-cell resolution by analyzing their single-cell transcriptomes paired with the T cell antigen receptor (TCR) repertoires. The hCMV-reactive T cells were highly heterogeneous and consisted of different developmental and functional memory T cell subsets such as, long-term memory precursors and effectors, T helper-17, T regulatory cells (T_{REGs}) and cytotoxic T lymphocytes (CTLs) of both CD4 and CD8 origin. The hCMV-specific T_{REGs}, in addition to being enriched for molecules known for their suppressive functions, showed enrichment for the interferon response signature gene sets. The hCMV-specific CTLs were of two types, the pre-effector and effector-like. The co-clustering of hCMV-specific CD4-CTLs and CD8-CTLs in both pre-effector as well as effector clusters suggest shared transcriptomic signatures between them. The huge TCR clonal expansion of cytotoxic clusters suggest a dominant role in protective immune response to CMV.

Conclusions

The study uncovers the heterogeneity in the hCMV-specific memory T cells reveling many functional subsets with potential implications in better understanding of hCMV-specific T cell immunity. The data presented can serve as a knowledge base for designing vaccines and therapeutics.

Background

The acquisition of immunological memory to infections is the hallmark of protective immune response. During this conserved process of T cell immunological memory development, the naive T cells that have not previously encountered antigen, differentiate during the primary infection, into memory T cells that have specialized functions in immune defence to a subsequent infection with the same pathogen. A small number of antigen-specific memory T cells can have an enormous impact in directing or misdirecting an immune response upon secondary infection. However, the rarity of antigen-specific memory T cells have limited the detailed characterization of these cells until very recently. The utilization of single-cell genomics to dissect the heterogeneity and understand th global gene expression patterns of these rare antigen-specific memory T cells has advanced our understanding of various disease-specific T cell memory repertoire in an unbiased manner [1-7].

$CD4^+$ memory T cells are classified based on their functional properties and in addition more recently also based on their transcriptomes, into multiple subsets such as but not limited to, T helper (T_H)1, T_H2, T_H17, $T_H1/17$, T follicular helper (T_{FH}), and T regulatory (T_{REG}) cells [8-12]. For example, T_{FH} cells are the specialized providers of help to B cells, and T_{REGs}, the regulators of the immune response with their immunosuppressive properties [11, 13, 14]. Furthermore, each of those subtypes can exhibit great functional diversity and plasticity [12]. The peripheral $CD4^+$ as well as $CD8^+$ memory T cells can also be classified based on their developmental stages as long-lived precursor memory and short-lived effector memory T cells such as, stem cell memory T cells (T_{SCM}), central memory T cells (T_{CM}), and effector memory T cells (T_{EM}), effector memory T cells expressing CD45RA (T_{EMRA}) [15]. The $CD8^+$ T cells are known for their cytotoxic functions, and the $CD4^+$ T cells, predominantly, for their helper function where they provide help to other immune cell types including the $CD8^+$ T cells in resolving the infection. However, others and we have shown that $CD4^+$ T cells can also function

71 as cytotoxic T cells and are enriched in the CD4-T_{EMRA} compartment and show marked T cell
72 antigen receptor (TCR) clonal expansion similar to the CD8-T_{EMRA} cells in many acute and
73 chronic viral infections including the cytomegalovirus (CMV) [1, 3, 4, 6, 16-22].

74 Following initial infection, the human CMV (hCMV) establishes persistence or latency
75 in immune-competent individuals, although intermittent viral shedding can occur [23]. In the
76 absence of an effective immune response especially in immune-compromised individuals, the
77 virus can reactivate and cause the disease. Hence, reactivation of hCMV poses a higher risk for
78 individuals undergoing transplant or chemotherapy, immune-compromised Human
79 Immunodeficiency Virus (HIV) infected individuals, and new-borns of hCMV seropositive
80 mothers [23]. Both $CD4^+$ and $CD8^+$ T cells have been shown to play important roles in the
81 immune response to CMV [24, 25]. While hCMV-specific $CD8^+$ T cells have extensively been
82 studied, studies on $CD4^+$ T cells are sparse [2]. Considering that the emergence of the hCMV-
83 specific $CD4^+$ T cells precedes that of $CD8^+$ T cells, they were mostly thought to perform
84 supportive roles by enhancing the $CD8^+$ T cell responses to the hCMV infection. However,
85 subsequent studies have demonstrated additional roles of CD4+ T cells, other than the
86 supportive one towards $CD8^+$ T cell, in CMV immunity (reviewed in [2]). The poorer or lack
87 of hCMV-specific $CD4^+$ T cell responses have been associated with persistent viral shedding
88 in urine and saliva as well as severe disease outcomes [24-27]. In individuals undergoing stem
89 cell or organ transplantation, hCMV-specific $CD4^+$ and $CD8^+$ T cells have been shown to
90 abrogate reactivation [25-29]. Further, during the primary infection, the role of $CD4^+$ T cells
91 has been established in resolution of the disease symptoms [30, 31]. The identification of
92 hCMV-specific T cells has classically relied on the measurement of intracellular cytokine
93 production, predominantly interferon gamma (IFNγ) and to a lesser extent interleukin 10
94 (IL10), in response to stimulation with peptides derived from various hCMV ORFs (Open
95 Reading Frame) or total viral lysate [2, 6, 16, 32-35]. Several studies, in healthy seropositive

individuals, have identified a higher percentage of hCMV-specific T cells, reaching almost as high as ~5-10% of total $CD4^+$ and $CD8^+$ T cells for epitopes derived from pp65 and IE-1 proteins of hCMV, with majority of them showing terminally differentiated effector memory phenotype [16, 33, 34]. In addition to producing IFNγ, the hCMV-reactive $CD4^+$ T cells have been shown to make cytolytic molecules such as Granzymes, Perforin, and CD107a (degranulation marker), and showed efficient lysis of hCMV infected dendritic cells and controlled virus dissemination *in vitro*, suggesting prominent role of cytotoxic $CD4^+$ T cells in hCMV immunity [16-20]. $CD4^+$ T cells expressing CD25 and FOXP3 (T_{REGs}), producing IL10, an immunosuppressive cytokine, have also been observed and are implicated in immune suppression in CMV infection and reactivation [36-39]. However, a detailed characterization of the spectrum of hCMV-specific $CD4^+$ memory T cells with respect to their heterogeneity and molecular signatures have been lacking. Hence, the identification and characterization of the overall hCMV-specific memory T cells with respect to their molecular signatures, in CMV seropositive individuals who are otherwise healthy, will enable the identification of correlates of protective immune response to hCMV.

Hence, in this study, to isolate the spectrum of hCMV-specific T cells, independent of their cytokine profile and Human Leukocyte Antigen (HLA) restriction or not limited to a single peptide (peptide-MHC multimers), we used ARTE (Antigen-Reactive T cell Enrichment) assay [40, 41]. The ARTE assay utilizes the surface expression of co-stimulatory molecules (CD154 and CD137) upon TCR engagement with cognate peptide-MHC (Major Histocompatibility Complex) complex [40, 41]. To dissect the heterogeneity across T cell memory subsets and TCR clonal diversity of hCMV-specific memory T cells, we isolated and performed single-cell transcriptomics analysis of over 8000 hCMV-specific memory T cells, isolated based on the surface expression of $CD154^+$ and/or $CD137^+$ across 10 seropositive donors, after stimulation with pool of hCMV peptides derived from T cell immuno-dominant

121 epitopes of pp65 and IE-1 proteins. Unbiased clustering based on single-cell transcriptomes
122 identified nine distinct clusters of various functional subsets including, T_{REGs}, T_H17, T_H1 and
123 $T_H1/17$, and cytotoxic $CD4^+$ T cells (CD4-CTLs). The hCMV-antigen specific T_{REGs} were
124 enriched for molecules linked to their suppressive function and interferon response genes
125 ($T_{REG\text{-}IFN}$). The transcriptomics analysis combined with TCR repertoire analysis revealed that
126 the cytotoxic cells are predominantly of 2 types; pre-effectors and effectors and are highly
127 clonally expanded. Interestingly, we observed that the transcriptomes of pre-effectors and
128 effectors of CD4-CTLs and CD8-CTLs were largely indistinguishable. Together, in an
129 unbiased approach, our study has identified many previously known as well as novel subsets
130 of hCMV-specific memory T cells and their unique transcriptomic signatures, which
131 potentially have implications in understanding the reactivation of hCMV in immune-
132 compromised individuals. This knowledge base can be an important resource for designing
133 vaccines and therapeutics.
134

135 **Results**

136 ***Single-cell transcriptomic analysis of CMV-specific memory T cells***

137 To identify and understand the heterogeneity and clonal diversity of the spectrum of hCMV-
138 specific T cells across different memory subsets in an unbiased way, we performed single-cell
139 transcriptomic (scRNA-Seq) and single-cell TCR (T Cell antigen Receptor) repertoire analysis
140 (scTCR-Seq) of >8000 hCMV-specific memory T cells (Fig. 1A and B). To isolate the
141 spectrum of hCMV-specific T cells independent of their cytokine profile and HLA restriction,
142 we utilized the widely used ARTE (Antigen-Reactive T cell Enrichment) assay where the
143 surface expression of co-stimulatory markers such as CD154 and CD137 is analysed upon the
144 engagement of T cell antigen receptor (TCR) with cognate pMHC (peptide Major
145 Histocompatibility Complex) complex [1, 3, 7, 40-42]. For single-cell omics experiments, we

146 isolated T cells using florescence activated cell sorting (FACS) based on the surface expression
147 of CD154 and CD137 upon stimulation of PBMCs (Peripheral Blood Mononuclear Cells) from
148 10 hCMV-seropositive and high peptide responder individuals with peptide pools derived from
149 immunodominant pp65 and IE-1 (Fig. 1A and Additional file 1: Fig. S1A-C). To compare the
150 hCMV-specific memory T cells across known memory subsets, the peptide responding T cells,
151 from different $CD4^+$ memory T cell compartments (naïve T cells (T_N; $CD45RA^+CCR7^+$),
152 central memory T cells (T_{CM}; $CD45RA^-CCR7^+$), effector memory T cells (T_{EM}; $CD45RA^-$
153 $CCR7^-$), and effector memory T cells expressing CD45RA (T_{EMRA}; $CD45RA^+CCR7^-$) [15]),
154 were FACS sorted separately and pooled before performing single-cell omics experiments (Fig.
155 1A and Additional file 1: Fig. S1B and C). Further, considering the enrichment of CD4-CTLs
156 (cytotoxic T lymphocytes) in the CD4-T_{EMRA} subset, to parallelly compare the hCMV-specific
157 CD4-CTLs and CD8-CTLs we also included hCMV-reactive T cells from CD8-CTL
158 compartments ($CD8^+CCR7^-$ (CD8-T_{EM} and -T_{EMRA})) in the single-cell omics experiments (Fig.
159 1A and Additional file 1: Fig. S1B and C) [4]. An unbiased clustering of 6899 hCMV-specific
160 memory T cells (out of 8062 cells) that passed our quality control parameters (QC; please see
161 methods section), identified 9 distinct clusters based on transcriptomes (Fig. 1B), and the
162 clustering was not influenced by donors or the experimental batch (Additional file 1: Fig. S1D
163 and E; Additional file 2: Table S1). Different developmental T cell memory subsets were
164 distinguished based on the surface expression of oligo-tagged antibodies (antibody derived
165 tags; adt) against CD45RA, CCR7, CD95 and IL7Rα as well as *CCR7*, *CD27*, *CD28* transcripts
166 (Fig. 1C and D; Additional file 2: Table S2) [4, 15]. Transcripts for *CD4* were distributed across
167 all clusters while *CD8B* transcripts were majorly found in clusters 2 and 4 (Fig. 1E). Cells in
168 cluster 2 and 4 were mostly T_{EMRA} cells of both CD4 and CD8 origin as they expressed
169 CD45RA (adt CD45RA) and lacked the expression of CCR7 protein (adt CCR7), as well as
170 transcripts for *CCR7*, *CD28* and *CD27* (Fig. 1C and D) [4, 15]. T_N cells were very few and

171 were mostly found in cluster 6 ($CD45RA^{+}CCR7^{+}IL7R\alpha^{+}$) (Fig. 1C and D). T_{CM} and T_{EM} cells
172 were distributed across multiple clusters (Clusters 0, 1, 3, 5, 6, 7) (Fig. 1C and D). These
173 observations were independently confirmed by the enrichment of subset-specific gene
174 signatures from T_{CM}, T_{EM}, and T_{EMRA}, as well as common gene signatures from T_{CM}-T_{EM}, and
175 T_{EM}-T_{EMRA} [4] (Fig. 1F; Additional file 1: Fig. S1F; Additional file 2: Table S3). Both CD4-
176 and CD8-T_{EMRA} cells (clusters 2 and 4) majorly showed higher expression of *CD137* while
177 other T_{CM} and T_{EM} clusters (0, 3, 6) showed higher expression of *CD154* (Fig. 1G).
178 Interestingly many of the T cell activation markers showed dynamic expression amongst the
179 clusters; *CD154* and *CD137* showed opposing expression and similar observations were made
180 for *CD69* and *IL2RA* (Fig. 1D and G). Further, co-expression analysis of various T cell
181 activation markers in combination, confirmed the variability in expression (Fig. 1G). Most
182 strikingly, the $CD137^{hi}CD154^{lo}$ cells showed low *CD69* expression, while the *CD154* and
183 *CD137* co-expressing cells expressed similar amounts of *TNFRSF4* transcripts (encoding
184 OX40) (Fig. 1G). Together, these results show that our data well represents various memory
185 subsets that show differential expression of T cell activation markers.

186 ***hCMV-specific memory T cells are heterogeneous and can be classified into multiple***
187 ***functional T cell subsets***

188 The differential expression analysis of transcripts amongst the nine clusters of hCMV-specific
189 T cells, identified cluster specific expression of transcripts, revealing many functional T cell
190 subsets (Fig. 2A and B; Additional file 2: Table S4). Multiple clusters showed enrichment for
191 long-term memory markers such as *AQP3*, *CCR7*, *TCF7*, *IL7R*, *LTB*, *JUNB, SELL* (Fig. 2A
192 and B) [3, 4]. Cluster 1 showed enrichment for *FOXP3*, *BATF*, *TIGIT* and *TNFRSF1B*
193 transcripts that are known to be expressed in T regulatory cells (T_{REG}) (Fig. 2B). Interestingly,
194 cluster 1 also showed enrichment of transcripts encoding interferon (IFN) response signature
195 genes (*ISG20*, *ISG15*, *IFIT3*, *OAS1*, *MX1*) (Fig. 2B). In an independent analysis, cluster 1 cells

196 showed a higher enrichment signature score for overall T_{REG} and IFN response signature gene
197 sets (Fig. 2C; Additional file 2: Table S3), suggesting that cells in cluster 1 are T_{REG} cells and
198 are possibly responding to IFN signalling ($T_{REG\text{-}IFN}$). Actively cycling cells were found in
199 cluster 3, one of the clusters enriched for T_{CM} signatures (Fig. 2B and C; Additional file 2:
200 Table S3) [43]. Cells in clusters 2 and 4, enriched for T_{EMRA}-specific gene sets, expressed
201 transcripts encoding cytolytic molecules such as *GZMB*, *PRF1* and *NKG7* and showed
202 enrichment for cytotoxicity gene signatures (Fig. 1F, Fig. 2B and C; Additional file 1: Fig.
203 S1F; Additional file 2: Tables S3 and S4) [4], suggesting that clusters 2 and 4 are cytotoxic
204 clusters. The presence of mixture of cells expressing *CD4* and *CD8* transcripts in both the
205 cytotoxic clusters 2 and 4 suggest possible similarities between CD4-CTLs and CD8-CTLs.

206 We next interrogated the single-cell transcriptome of hCMV-specific T cells for
207 functional T helper (T_H) cell subtypes such as T_H1, T_H17 and $T_H1/17$, that are known to have
208 role in viral infections [3, 44]. Multiple clusters showed expression of T_H subset-specific
209 transcripts: T_H17 (*CCR4*, *CCR6*, *IL4I1*, *CTSH*), T_H1 (*CXCR3*, *TNF*, *IFNG*, *CSF2*) and $T_H1/17$
210 (*CXCR3, DPP4*) [9, 10] (Fig. 2D; Additional file 2: Table S4). Interestingly, we found several
211 clusters co-expressing transcripts from different T_H subsets, suggesting each cluster may have
212 cells belonging to more than one T_H subtype. Independently, module enrichment analysis using
213 T_H subset-specific gene sets corroborated these results (Additional file 1: Fig. S2A; Additional
214 file 2: Table S3). The T_H1-specific gene sets were enriched in cluster 2 and 4, the cytotoxic
215 clusters (Additional file 2: Fig. S2A). Considering there are several overlapping genes between
216 T_H1 and cytotoxic gene sets, this observation is in alignment with the known literature [4, 9,
217 10]. T_H17 signature genes showed highest enrichment in cluster 0, followed by clusters 7, 3
218 and 1. $T_H1/17$ signatures were mostly enriched in cluster 0 followed by clusters 5 and 7
219 (Additional file 1: Fig. S2A) [9, 10]. Together these observations indicate that each hCMV-
220 specific T_H subset is at different developmental stages of the memory (long-term memory and

221 effector memory) and clustering was predominantly influenced by the developmental stages of
222 memory T cells

223 ***TCR clonally expanded hCMV-specific T cells are majorly observed in cytotoxic clusters.***

224 To understand the TCR clonal diversity amongst the hCMV-specific T cells we analysed the
225 single-cell TCR-Seq data generated from the same cells. We recovered TCRs from 83.56%
226 (5765 cells of 6899 cells) of the total QC-ed cells in our data set, of which 21.40% (1234 of
227 5765 cells) were clonally expanded (Fig. 2E; Additional file 2: Table S5). Several clusters
228 shared TCR clonotypes, indicating a shared developmental lineage between these clusters
229 (Additional file 1: Fig. S2B). A maximum of 14 clonotypes were shared between clusters 2 and
230 4, followed by clusters 0 and 3 sharing 10 clonotypes (Additional file 1: Fig. S2B). Cells in
231 cluster 2 and 4 showed highest clonal expansion with ~78% and ~76% of the cells being
232 expanded respectively (Fig. 2E; Additional file 2: Table S5). As high as 76% of the total
233 expanded cells (938 of 1234) were found in cluster 2 (50%) and cluster 4 (~26%) (Additional
234 file 2: Table S5). A few top expanded clonotypes were found in as many as 144, 79 and 51
235 cells from clusters 2 and 4, indicating the preferential expansion of a few specific clonotypes
236 (Fig. 2F; Additional file 1: Fig. S2C). Interestingly, close to 58% of the expanded cells carried
237 only 20 clonotypes (Fig. 2F). Both CD4-CTLs and CD8-CTLs (T_{EMRA}) are shown to be
238 clonally expanded in several diseases including CMV in both humans and animal models [2-
239 4, 45, 46]. Clonal expansion and enrichment for cytotoxic signature in clusters 2 and 4
240 emphasizes the role for cytotoxic cells in hCMV-specific protective immune response [16-20].

241 ***Single-cell transcriptome analysis of hCMV-specific T_{REG} cells***

242 T_{REGs} are characterised by the higher expression of CD25 (IL2RA) and the transcription factor
243 FOXP3, but a lower expression of IL7Rα (CD127) in humans [47]. CMV-specific T_{REGs} have
244 been reported in both mouse models and humans following primary infections and are shown
245 to produce IL10, a suppressive cytokine [2, 6, 36-39, 48-50]. However, the detailed molecular

246 signatures of hCMV-specific memory T_{REGs} have not been well described. The transcript
247 encoding the T_{REG} specific transcription factor FOXP3 was differentially expressed in clusters
248 1 (85% of cells) and 7 (Fig. 2B, Fig. 3A and B; Additional file 2: Table S4), however though
249 not differentially expressed, a portion of cells from cluster 5 showed higher *FOXP3* expression
250 (41% of cells), while various other clusters (clusters 0 and 3) showed lower levels of *FOXP3*
251 expression (Fig. 3A and B). Considering FOXP3 can be transiently expressed on TCR activated
252 cells, we examined the co-expression of other T_{REG} related genes and *FOXP3*. The cells co-
253 expressing *FOXP3* - *IL2RA*, and *FOXP3* - *IKZF2* were enriched in cluster 1 and portion of
254 cluster 5, and as expected they showed lower expression of IL7Rα (Fig. 1C and Fig. 3A) [47].
255 Clusters 1 and 5 were also characterized by the higher expression of other T_{REG}-specific
256 transcripts such as *TIGIT*, *BATF*, *TNFRSF1B* and the Ikaros Zinc Finger (IkZF) transcription
257 factor (TF) family members *IKZF1* encoding Ikaros, *IKZF2* encoding Helios, *IKZF3* encoding
258 Aiolos, *IKZF4* encoding Eos (Fig. 2B and Fig. 3C). The overall T_{REG} gene signature was
259 enriched in cluster 1 and fraction of cluster 5 (Fig. 2C). Together these results show that T_{REG}
260 cells are predominantly in cluster 1 and portion of cluster 5 and the cells from clusters 0 and 3
261 are potentially non-T_{REG} cells, transiently expressing low levels of *FOXP3* in response to TCR
262 activation. We next interrogated if the hCMV antigen-specific T_{REGs} in our data set were indeed
263 memory T_{REGs}. Based on the expression of CD45RA, the $FOXP3^{+}$ T_{REGs} have been classified
264 as resting or naïve T_{REGs} ($FOXP3^{lo}CD45RA^{+}$) and effector T_{REGs} ($FOXP3^{hi}CD45RA^{-}$) [51, 52].
265 Further the effector T_{REGs} have been classified as central and effector memory cells based on
266 the expression of CCR7, CD27 and CD28 [53]. The T_{REGs} in our data set were characterized
267 by the lack of expression of CD45RA, and a moderate expression of CCR7, *CD27* and *CD28*,
268 indicating that they are mostly central and effector memory T_{REGs} rather than naïve T_{REGs} (Fig.
269 1C and D).

270 Although, T_{REGs} expressing FOXP3, are known for their suppressive function, many
271 reports have shown the presence of T cells expressing FOXP3 transiently, in response to TCR
272 activation that are non-suppressive in nature. Hence, we assessed if the hCMV-specific T_{REGs}
273 in our data set are expressing markers associated with the suppressive nature of T_{REGs}. The
274 molecular signatures of T_{REGs} found in clusters 1 and 5 indicated their potential suppressive
275 nature, compared to cells expressing low levels of *FOXP3* observed in clusters 0 and 3 (Fig.
276 3A). The T_{REGs} in clusters 1 and 5 were $CD137^{+}CD154^{lo}$, the activation induced characteristic
277 of T_{REGs} implicative of epigenetically stable antigen-activated T_{REGs} that retain the high
278 suppressive potential in humans after *in vitro* or *ex vivo* activation (Fig. 1D and G) [54]. The
279 T_{REGs} in clusters 1 and 5, showed higher expression of *TIGIT*, *TNFRSF18* (GITR) and *CTLA-*
280 *4*, genes that are associated with T_{REGs} containing high affinity TCRs, further suggesting their
281 antigen-specificity (Fig. 2B and Fig. 3C). The T_{REGs} in clusters 1 and 5 also showed higher
282 expression of *ENTPD1* (CD39), an ectoenzyme ATP apyrase, *CCR4*, *CTLA4*, Helios (*IKZF2*)
283 and FAS (CD95), molecules that are reported to be associated with effector and suppressive
284 function (Fig. 1C, Fig. 2D and Fig. 3C) [55-57]. A suppressive function of Helios in T_{REGs} has
285 been suggested, where $Helios^{+}FOXP3^{+}$ T_{REG} cells produced lower amounts of $T_{H}17$-specific
286 cytokine, IL17, compared to $Helios^{-}FOXP3^{+}$ T_{REG} cells, hence promoting the formation of
287 T_{REGs} rather than $T_{H}17$ subtype [57]. Consistent with these observations, we found that clusters
288 0 and 3 that expressed *IL17F* and *IL17A*, expressed low levels of *FOXP3*, but lack the
289 expression of *IKZF2* (Helios) and these cells showed higher expression of *CD154* and lower
290 expression of *CD137* (Fig. 2B, Fig. 3A andC) [54, 57]. Together these observations suggest
291 that the low *FOXP3* expressing cells in clusters 0 and 3 are potentially the induced/transient
292 T_{REGs} that are possibly expressing FOXP3 transiently in response to activation and are non-
293 suppressive in nature. Conversely, T_{REG} cells in cluster 1 and 5 are $Helios^{+}FOXP3^{+}$, and did
294 not express *IL17A* and *IL17F*, indicative of suppressive nature (Fig. 2B, Fig. 3A and C). The

295 lack of expression of exhaustion markers *PDCD1* and *LAG3* further suggests these are not
296 associated with anergy or exhaustion (Fig. 3C). Together these results provide multiple
297 evidences to suggest that the T_{REGs} in clusters 1 and 5 are effector memory T_{REGs} and are
298 potentially suppressive in nature. One of the mechanisms through which T_{REGs} execute their
299 suppressive function on effector T cells is through cytokines such as IL10, TGFβ and IL35
300 (reviewed in [58]). The T_{REGs} in cluster 1 lacked or showed low expression of these suppressor
301 cytokine transcripts *TGFB1*, *IL10* and *IL35*, indicating that cells in cluster 1 may not be actively
302 suppressing the hCMV-specific effector T cells, at least in the experimental setting used in the
303 study (Fig. 3C; Additional file 2: Table S4).

304 We next interrogated if the T_{REG} subsets in our data set, that showed enrichment for
305 molecules linked to their suppressive function, are not suppressive towards hCMV-specific
306 effector T cells, then which cell types are they targeting in hCMV-specific immunity. Studies
307 using mouse models have shown that T_{REGs} can show remarkable functional plasticity and
308 execute their suppressive function by expressing the TF and the chemokine receptor of the
309 target T_H subtypes [14, 59-62]. For example, the T_{REGs} suppressive towards T_H1 will express
310 T-bet (encoded by *TBX21*) and CXCR3 (T_H1-T_{REGs}), while the ones toward T_H2 will express
311 GATA3 and CCR4 (T_H2-T_{REGs}), albeit at a reduced level compared to the T_H subtype itself,
312 without necessarily themselves making the T_H subtype-specific cytokines [14, 60-62].
313 Interestingly the differential gene expression analysis revealed that the T_{REGs} in cluster 1 and
314 5, are characterized by the higher expression of T_H2-specific TF *GATA3* and chemokine
315 receptor *CCR4* along with *FOXP3* (Fig. 3D-F). GATA3 has been shown to be important for
316 FOXP3 expression and T_{REG} functions [61]. Hence, we independently examined the overall
317 T_H2 subset-specific gene signatures using module enrichment score and gene set enrichment
318 analysis (GSEA). We found that both cluster 1 and 5 are enriched for T_H2 subset-specific gene
319 signatures (Fig. 3G and H), suggesting the T_{REGs} in cluster 1 and 5 are most probably T_H2-like

320 T_{REGs}. A recent study that analysed the T cells in pan cancers has also shown the presence of
321 T_H2- like T_{REGs} that were marked by a higher expression of *GATA3* [63]. Clusters 1 and 5 were
322 also characterised by the enrichment of IFN response signature genes ($T_{REG\text{-}IFN}$) (Fig. 2B and
323 C). In asthma and house dust mite allergy, both T_H and T_{REG} subsets enriched for IFN response
324 gene sets showed dampened T_H2 response in healthy individuals with no prior history of allergy
325 or asthma [5]. Interestingly, in our data set, a joint enrichment analysis using the house dust
326 mite allergy-specific T_{REG} gene signature and T_H2-specific gene signature showed enrichment
327 in cluster 1 and 5 (Fig. 3I) [5]. Together these results suggest that T_{REGs} in clusters 1 and 5 are
328 likely T_H2-T_{REGs} with IFN response signatures that are potentially suppressive towards T_H2.
329 The T follicular regulatory cells (T_{FRs}) suppress T_{FH} responses and are characterized by the
330 expression of IL1R2 and CCR8 [3, 64, 65]. The hCMV-reactive T_{REG} cells in clusters 1 and 5
331 co-expressed *IL1R2* and *CCR8* transcripts along with *FOXP3* transcripts, hence, may represent
332 T_{FR} cells (Fig. 3D-F) [3, 64, 65]. These interesting observations warrant further investigation
333 to understand the relevance of T_H2-T_{REGs} and T_{FRs} in CMV immunity, especially when hCMV-
334 reactive conventional (non-T_{REGs}) T_H2 and T_{FH} cells were absent in our data set.

335 ***hCMV-reactive CD4-CTLs and CD8-CTLs show similar transcriptomic profile***

336 Majority of the cells in clusters 2 and 4 and fraction of cells in clusters 0 and 7 were
337 characterized by the high expression of transcripts encoding cytolytic molecules such as
338 Granzyme B (*GZMB*), Perforin (*PRF1*), Granulysin (*GNLY*), and transcription factors *HOPX*
339 and *ZEB2* and showed enrichment for cytotoxicity and T_{EMRA}-specific signature genes (Fig.
340 1F, Fig. 2B and C, Fig. 4A and B) [3, 4, 16-20]. Interestingly, these cytotoxic clusters could
341 not be differentiated based on the expression of *CD4* or *CD8A* and *CD8B* transcripts, but by
342 other cytotoxicity related molecules (Fig. 1E and Fig. 4A-C). The cytolytic granules have been
343 shown to contain chemokines such as CCL3, CCL4 and CCL5 in addition to the classical
344 mediators of cytotoxicity (GZMB, PRF1, GNLY), in both viral and bacterial infections,

345 indicating their role in cytolysis [66, 67]. Cells in cluster 2 showed higher expression of the
346 transcripts encoding the cytokines such as *TNF* and *IFNG*, chemokines such as *CCL3*, *CCL4*,
347 *CCL4L2*, *XCL1*, *XCL2*, while cluster 4 showed higher expression of *CCL5* (Fig. 4B and C).
348 The chemokine receptor *CCR5*, the receptor for chemokines *CCL3*, *CCL4* and *CCL5*, and
349 *IFNGR1*, encoding the receptor for IFNG, was expressed by the cytotoxic cells in cluster 0,
350 suggesting these cells may be responding to the cytokines and chemokines made by the cells
351 in cytotoxic clusters 2 and 4 and are potentially the intermediate population (Fig. 4A and B;
352 Additional file2: Table S4) [68]. This is further supported by the single-cell trajectory analysis,
353 where on the pseudo time scale cluster 0 appears before clusters 2 and 4 (Fig. 4D). These results
354 suggest that the cytotoxic cells in cluster 0 are potentially an intermediate population in the
355 CTL lineage and these cells are mostly T_{EM} cells as they mostly lack the expression of CD45RA
356 and CCR7 (Fig. 1C).

357 Compared to cluster 4, cluster 2 cells showed higher expression of *SLAMF7*, *ZEB2*,
358 *GZMB*, *GPR18*, *CD72*, *PDCD1* (PD1), *CRTAM* that are known to be expressed in terminally
359 differentiated effector cells in viral infections and various cancers [3, 69-72] (Fig. 2B, Fig. 3C,
360 Fig. 4B and D). On the contrary, cluster 4 was characterized by the higher expression of *GNLY*,
361 *EOMES*, *ADGRG1* (GPR56), *KLRD1*, *UCP2* and *CRIP1* (Fig. 2B, Fig. 4B and D), that are
362 mostly not associated with terminally differentiated effector T cells. For example, CRIP1 has
363 been shown to be anti-apoptotic in cancers and the antigen-specific cells expressing UCP2
364 survive better in HIV infection through metabolic reprogramming [73, 74], suggesting the
365 possible role of these genes in providing survival advantage to cells in cluster 4. A coordinated
366 expression of CCL5 followed by GNLY and PRF1 provided host-defence against
367 *Mycobacterium tuberculosis* (Mtb) infection, where the expression of CCL5 attracted the Mtb
368 infected macrophages that in-turn triggered the expression of GNLY and PRF1 in CD8 T cells
369 [75]. Further, a delayed onset of cells expressing GNLY has been shown in multiple infections

370 [76, 77]. These results suggest that the cytotoxic cells could be at different stages of their
371 development or effector function. The differential expression of many of these cytolytic
372 molecules between clusters 2 and 4, imply that the cells in cluster 2 are potentially the terminal
373 effector cells while those in cluster 4 are pre-effector cells. This observation is further
374 strengthened by the TCR analysis (Fig. 2E and F, Fig. 4E and F; Additional file 1: Fig. S2B
375 and C). The 20 most expanded clonotypes were found majorly in cluster 2 and 4 (Fig. 2F;
376 Additional file 1: Fig. S2C). Cluster 2 is relatively more clonally expanded than cluster 4,
377 where over 67% of the cells harbouring the 20 most expanded clonotypes were found in cluster
378 2 (Fig. 4F). The trajectory analysis also showed that on a pseudo-time scale, cluster 2 and 4
379 appears to bifurcate from a common origin of cluster 0 (Fig. 4D). Further, the pathway
380 enrichment analysis of genes differentially expressed between clusters 2 and 4 revealed an
381 enrichment for cytokine and chemokine response pathways in cluster 4, while cluster 2 showed
382 enrichment of pathways associated with pathogen induced cytokine storm (Additional file 1:
383 Fig. S3A and B). The effector T cells utilize glycolysis, as the preferred metabolic pathway
384 that play an important role for cytokine secretion and lytic nature of these effector cells [78-
385 80]. The cells in cluster 2 showed enrichment for many metabolic pathways associated with
386 effector cells such as glycolysis and HIF1α signalling as well as pathways related to anti-viral
387 responses (Additional file 1: Fig. S3A). Together, these combined analysis of the
388 transcriptome, TCR clonotype expansion and sharing along with the trajectory analysis
389 provides the evidence to support the idea that cluster 4 cells are pre-effectors while cluster 2
390 cells are effectors.

391 Next to assess if the observed differences between the CTL clusters 2 and 4 are
392 influenced by the proportion and the characteristics of CD4-CTLs and CD8-CTLs, we
393 compared the expression of these transcripts between CD4 and CD8 T cells within clusters 2
394 and 4. The proportions of CD4 and CD8 T cells within clusters 2 and 4 were comparable (Fig.

395 4G), indicating that the disproportionate distribution of $CD4^+$ and $CD8^+$ T cells is not the cause
396 of the observed differences between clusters 2 and 4. Overall, the transcriptome profile of CD4,
397 CD8 or cells that could not be assigned as CD4 or CD8 T cells (NA) within each cluster did
398 not vary except for *CD8A* and *CD8B* transcripts (Fig. 4H and I). Transcripts such as *PRF1* and
399 *NKG7* that showed comparable expression between cluster 2 and 4, followed the same pattern
400 even when these two clusters were further sub-divided based on the CD4 and CD8 T cell sub-
401 type. The transcripts that showed higher expression in cluster 2 (*XCL1*, *ZEB2*, *CRTAM* and
402 *GZMB*) and cluster 4 (*CCL5*, *GNLY*, *EOMES*), followed similar pattern of expression in CD4
403 and CD8 T cells within each of these effector and pre-effector clusters (Fig. 4H and I). Both
404 CD4 and CD8 T cells from cluster 4 showed higher expression of IFN response genes *ISG20*
405 and *IFI6* while those in cluster 2 showed higher expression of cytokines *TNF* and *IFNG* (Fig.
406 4H and I). We observed that the cells in clusters 2 and 4 have distinct gene expression pattern
407 that is not influenced by either CD4 or CD8 T cell proportion (Fig. 4H and I). Overall, our data
408 has revealed that both hCMV-reactive CD4-CTLs and CD8-CTLs share similar transcriptome
409 profile and can be classified as effectors and pre-effectors of CTLs.
410

411 **Discussion**

412 A significant world population carries the latent hCMV infection, without showing any
413 symptoms or causing the disease. However, latent infection poses a huge risk of reactivation
414 in immune-compromised individuals such as those undergoing transplant or infants born to
415 hCMV seropositive mothers. Although there is very little risk of the disease occurrence in
416 immune-competent individuals, the latent CMV infection puts a huge burden on the immune
417 system, especially for the elderly, where significant proportions of the T cells are found to be
418 hCMV-specific [46]. Identifying and understanding the characteristics of the hCMV-specific
419 T cell immune memory components in individuals carrying the virus in latent form,

420 representing protective immune response, can be of high value to design therapy or vaccines
421 to control CMV infection upon reactivation or maternal to fetal transfer.

422 Our understanding of *ex vivo*, antigen-specific human T cell responses to pathogens
423 such as hCMV remains limited, due to the rarity of the cells, the complexity of the biology,
424 and technical challenges of identifying overall antigen-specific $CD4^+$ memory T cells, since
425 they can be extremely heterogeneous in the expression of activation associated markers and
426 cytokines. An added layer of complexity comes from HLA-restriction of individuals and the
427 prior knowledge about the immune-dominant peptide, limiting the use of pMHC multimers.
428 Most studies have focused on isolating the total $CD4^+$ or $CD8^+$ T cells reactive to hCMV,
429 without considering the differences in memory proportions that can inadvertently bias the
430 analysis towards analysing the predominant memory compartment within $CD4^+$ T cells (T_{CM}
431 or T_{EM}) and $CD8^+$ T cells (T_{EMRA}). Our strategy to isolate antigen-specific T cells based on the
432 combination of TCR activation dependent markers (CD154 and CD137) across different
433 memory subsets followed by high resolution single-cell RNA-Seq paired with single-cell TCR
434 analysis allowed us to interrogate and compare a larger pool of hCMV (pp65 and IE-1)-reactive
435 cells from different memory subsets across 10 seropositive and peptide-responsive donors. This
436 unbiased approach enabled us to overlay the heterogeneity in T cell memory subsets classified
437 based on developmental stages and functional subsets along with their TCR dependent
438 activation markers. The expression of CD154 and CD137 in different set of cells that further
439 differentially co-expressed one or more T cell activation associated markers such as CD69,
440 CD25, OX40, warrants for careful selection of activation markers while analysing antigen-
441 specific cells *ex vivo*. In this study, we observed that though activated (based on the expression
442 of *CD154*, *CD137*, *CD69*, *CD25*, *OX40*), most cells, with the exception of effector cells, did
443 not actively make cytokines and those that made also showed heterogeneity for the cytokine

444 profile. Many studies previously have also relied on cytokine profiles to analyse *ex vivo* isolated
445 antigen-specific cells and hence have mostly analysed effector memory T cells.

446 The single-cell RNA-Seq of a large number of hCMV reactive cells isolated from 10
447 different donors, identified several interesting functional subsets; T_H17, T_{REGs}, CD4-CTLs and
448 CD8-CTLs. Of particular interest were CD4- and CD8-CTLs, that clustered together. The two
449 cytotoxic clusters observed could not be distinguished based on the CD4- and CD8-T cell
450 specific transcripts *CD4* or *CD8A*/*CD8B*, but on the basis of other cytotoxic molecules that
451 were linked to different states of effector functions [72]. The cluster that was predominantly
452 making cytokine and chemokine (*IFNG*, *TNF*, *XCL1*, *XCL2*, *CCL3*, *CCL4*) also expressed
453 transcription factor (TF) *ZEB2*, the TF known to be associated with late effector function [4,
454 72]. The cytotoxic cells in both clusters 4 and 0 appeared to respond to the cytokines and
455 chemokines by expressing their receptors (*IFNGR1*, *CCR5*). However, the cytotoxic cells
456 across these clusters expressed molecules linked to cytolytic granules (*PRF1*, *GZMB*, *GNLY*),
457 and transcription factor *HOPX*. The differential expression of many of the molecules linked to
458 cytotoxicity and effector functions, suggests the effector and pre-effector like subsets. These
459 subsets, possibly at different developmental states, might exist to ensure a continuity in immune
460 response during the entire course of the infection.

461 Another interesting discovery in our data set is the identification of T_{REGs} with
462 suppressive ability that showed enrichment for the IFN response gene signatures ($T_{REG\text{-}IFN}$)
463 which has been shown to be associated with a dampened T_H2 response in allergy [5]. The
464 enrichment of T_H2 signatures as well as the expression of *GATA3* and *CCR4*, the T_H2 associated
465 transcription factor and chemokine receptor by the T_{REGs} further suggested that these could be
466 suppressive towards the T_H2 subset. Although a very recent study in pan cancer has also
467 identified this subset, to the best of our knowledge, presence of T_{REGs} enriched for IFN response
468 genes has not been reported earlier in viral infections in humans [63]. Based on these

469 observations, we hypothesize that during the initial stages of the infection where the expansion
470 of effector cells is necessary, T_{REGs} may not be executing their suppressive function towards
471 these effectors, instead, suppressing other subtypes of no relevance to the disease. However,
472 further kinetic studies in both animal models and longitudinal human cohorts of different types
473 of diseases such as viral and bacterial infections, allergy and cancers are necessary to verify or
474 refute this hypothesis.
475

476 **Conclusion**

477 In conclusion, using the single-cell multi-omics approach (transcriptome, TCR repertoire and
478 expression of a few selected proteins), our study has identified an unprecedented amount of
479 heterogeneity in hCMV-specific $CD4^+$ memory T cell subsets. The study identified novel
480 subsets such as $T_{REG\text{-}IFN}$ and pre-effectors and effectors of both CD4-CTLs and CD8-CTLs.
481 The knowledge base can serve as an important resource for designing vaccines and therapeutic
482 strategies to control CMV infections, especially in immune-compromised individuals and
483 infants of seropositive mothers.
484

485 **Materials and Methods**

486 ***Study subjects***

487 Study subjects were healthy adult donors who donated blood at the Safdarjung Blood Bank
488 during 2019-20. The donors consented for use of the plasma and buffy coat samples for
489 research. Donors were HIV-negative and had no history of Hepatitis C infection. The median
490 age was 30.5 (24-39) and all these donors were male. Approval for the use of this material for
491 research was obtained from the institutional human ethics committees from both National
492 Institute of Immunology, New Delhi and Vardhman Mahavir Medical College (VMMC) and
493 Safdarjung Hospital, New Delhi, India.

494 ***PBMC processing***

495 Peripheral Blood Mononuclear Cells (PBMCs) were isolated from buffy coat samples from
496 healthy blood donors obtained from Safdarjung hospital blood bank by density gradient
497 centrifugation using Ficoll-Paque Premium (GE Healthcare Biosciences). PBMCs were
498 cryopreserved in 90% Fetal Bovine Serum (FBS) supplemented with 10% di-methyl sulfoxide
499 (DMSO).

500 ***CMV IgG analysis***

501 ELISA (Enzyme Linked Immunosorbent Assay) was performed on the plasma samples from
502 the donors obtained from the blood bank using Human Anti-Cytomegalovirus IgG ELISA kit
503 (abcam, #ab108724) according to the manufacturer's protocol to check for the donors' sero-
504 status. Donors with the absorbance values at least 10% higher than that of the cut-off control
505 supplied in the kit, were considered positive. Based on this criteria we found 124 out of 126
506 donors in our cohort were hCMV IgG+; 98.4% positivity) (Additional file 1: Fig. S1A).

507 ***PBMC stimulation***

508 To analyse or isolate antigen-specific T cells, the ARTE assay was employed with few minor
509 modifications [40, 41]. The hCMV-specific PepTivators (Miltenyi Biotec) derived from pp65
510 (UL83) and IE-1 (UL123) were used to stimulate PBMCs from CMV-seropositive donors,
511 according to the manufacturer's protocol. Briefly, PBMCs were thawed and treated with 50
512 U/mL Benzonase (Sigma) in RPMI before resting overnight in serum-free TexMACS medium
513 (Miltenyi Biotec) supplemented with 1% Penicillin/Streptomycin at 37°C in a 96-well plate.
514 Cells were stimulated for 6 or 24hrs at a density of 1 million/100 µL/well of 96 well plate, by
515 the addition of hCMV peptide pools (pp65 and IE-1 PepTivators) at a final concentration of 1
516 µg/mL in the presence of a blocking CD40 antibody (1 µg/mL; Miltenyi Biotec) and CD28
517 antibody (1 µg/mL; eBioscience) [1, 40, 41]. Stimulation with αCD3/CD28 DynaBeads Human
518 T cell activator (Invitrogen) (cell to bead ratio of 1:1) served as positive control while with

519 water (vehicle control) served as unstimulated negative control. The stimulated cells were
520 washed and stained with cocktail of fluorescent antibodies (Table S2A) and analysed by flow
521 cytometry or processed for single-cell RNA-sequencing using 10X genomics as follows. The
522 hCMV-peptide pool stimulated cells from each donor were washed and individually stained
523 with Cell-hashtag (HTO:Hash Tag Oligo) TotalSeq C antibody (0.5 µg/condition; Biolegend,
524 Table S2B) as per manufacturer's recommendations for 30 minutes on ice, and washed twice
525 with MACS buffer (PBS + 2% FBS + 2mM EDTA). HTO stained PBMCs from all 10 donors
526 were then pooled and stained with oligo-tagged TotalSeq C antibody for cell surface proteins
527 for T cell memory markers (CD45RA, CCR7, CD95 and IL7Rα) (0.5 µg/condition; Biolegend,
528 Table S2B) for 30 minutes on ice. Following washing, the pooled cells were further stained
529 with fluorescence-conjugated surface antibodies to enable FACS sorting of antigen-specific
530 cells (Table S2A). Cells were directly FACS sorted without an intermediate MACS column
531 enrichment step using FACSAria Fusion Cell Sorter (Becton Dickinson) in LoBind 1.5 mL
532 microcentrifuge (Eppendorf) tubes with 1:1 FBS:PBS supplemented with recombinant RNase
533 inhibitor (1:100, Takara). The live singlet gated CD3+ T cells were further gated as per the
534 gating strategy shown in additional file 1: Fig. S1B. List of antibodies used are provided in
535 additional file 2: Table S2. The flowcytometry data was analysed using FlowJo software
536 (v10.8).

537 ***Single-cell RNA-Seq***

538 The sorted antigen-specific cells from various memory compartments were pooled in desired
539 ratios and used for single-cell RNA-Seq and TCR-Seq assay using 10X Genomics kit, 5′ V(D)J
540 with gene expression and cell surface protein expression v1.1 as per the manufacturer's
541 recommendations. Initial amplification of cDNA libraries and final libraries were performed
542 for 15 cycles and 14 cycles respectively for gene expression library. V(D)J and cell surface
543 protein libraries were generated corresponding to each 5′ gene expression library using 9 cycles

544 of amplification. Libraries were sequenced on Illumina NovaSeq6000 sequencing platform for
545 paired end (PE)150 reads.

546 ***Single-cell RNA-Seq analysis***

547 Sequenced reads from the 5′ single-cell gene expression and associated V(D)J library were
548 mapped to the GRCh38 reference genome using 10X Genomics' cellranger multi (v6.1.1). The
549 cell surface protein quantification was run as part of the same pipeline. The Seurat package
550 (v4.3) in R (v4.2.2) was used to perform all further downstream analyses [81].

551 For downstream analysis, only cells that passed the QCs were retained; cells with UMI
552 (Unique Molecular Identifier) counts >500, number of genes >350 and percent mitochondrial
553 genes <15% were considered as good quality cells. Further, cells were assigned as doublets,
554 singlets or negatives based on the HTO counts using Demux with default parameters in Seurat
555 package (v4.3) [82]. Singlets were assigned to their respective donor based on HTO count.
556 Doublets were removed from downstream analysis. After applying all the quality control
557 parameters, we retained 6899 cells out of 8062 cells for downstream analysis (85.57% cells
558 passed the quality parameters). Cells from experiment 1 (3 donors) and experiment 2 (10
559 donors) were combined using the Seurat package after applying the QCs (Table S1).

560 For each cell, normalized UMI counts for each gene were obtained by dividing the raw
561 counts by the total counts across all genes. This was multiplied by a scaling factor of 10,000
562 and log transformed to yield the final normalized values. Prior to clustering, we filtered genes
563 by selecting for the top 2000 with highest variance across cells, using *FindVariableFeatures*
564 with *selection.method*="*vst*". This data was then centered and scaled using *ScaleData*, and the
565 top 50 principal components (PCs) were calculated. Top 18 PCs were selected using *ElbowPlot*
566 and *JackStrawPlot* for downstream processing. This was used to build a shared nearest
567 neighbour graph using *FindNeighbors*. The cells were clustered using *FindClusters*, with
568 *algorithm=3* and *resolution=0.2*, determined using the *clustree* function. For visualization and

569 clustering, a 2D UMAP projection of the top 18 PCs was obtained using the *RunUMAP*
570 function, with *metric="euclidean"* [81].

571 The cell surface protein tag data was normalized using the *NormalizeData* function in
572 Seurat with *normalization.method*="CLR". Briefly, for each cell, the hashtag counts were
573 divided by the geometric mean of counts of all unique hashtags prior to log transformation.

574 ***Differential gene expression analysis***

575 We identified differentially expressed genes using the MAST algorithm integrated within
576 Seurat's *FindAllMarkers* function using default parameters on $\log_2$(CPM+1) counts [81].
577 Genes in a cluster were reported as differentially expressed (DE) compared to every other
578 cluster if their $\log_2$ fold change of expression was > 0.25 and BH-adjusted P-value was < 0.05.

579 ***Gene module signature scores and Gene Set Enrichment Analysis (GSEA)***

580 Gene module scores were computed using the *AddModuleScore* function in Seurat, with default
581 parameters [81]. Briefly, for each cell, the module score is defined by the mean of the signature
582 gene list (test set) after subtracting the mean expression of an aggregate of control gene lists.
583 Control gene lists (same number as test gene list) are sampled from bins created based on the
584 level of expression of the signature gene list. GSEA was performed using Qlucore Omics
585 Explorer 3.8 software package [83]. List of the genes used are provided in supplementary table
586 S3.

587 ***Trajectory inference***

588 Single cell trajectories were computed using the slingshot algorithm within the dynverse/dyno
589 (v0.1.2) suite of trajectory inference pipelines [84]. Raw and normalized UMI counts from cells
590 of clusters 0, 2, 3, 4 and 7 were combined using the dynverse's wrap_expressions function.
591 Cells were assigned groups by cluster and the number of expected start and end states were set
592 to 1 using *add_prior_information*. Trajectory inference was run using *infer_trajectories* with

593 default parameters, with method = ti_slingshot(). We did not specify any start or end cells for
594 the trajectory.

595 ***Pathway enrichment analysis***

596 DE genes between clusters 2 and 4 were fed to Ingenuity Pathway Analysis software from
597 Qiagen. Enrichment pathways were sourced from Ingenuity core enrichment pathways.

598 ***TCR analysis***

599 For each cell, all information about clonality, expressed TCR chains, their sequences and
600 corresponding UMI counts were obtained as part of the standard 10X Genomics' cellranger
601 multi pipeline (Table S5).

602 ***Assigning CD4 and CD8 T cells***

603 For cells in cluster 2 and 4, we assigned cells as $CD4^+$ T cells, or $CD8^+$ T cells, first based on
604 the *CD4* and *CD8A*/*CD8B* transcript counts. Cells with > 0 counts for *CD4*, were assigned as
605 $CD4^+$ T cell (333 cells). For $CD8^+$ T cells, we considered the cell as $CD8^+$ T cell (735 cells) if
606 the sum of all three CD8 transcripts (*CD8A*, *CD8B*, *CD8B2*) was > 0 and *CD4* transcripts were
607 undetectable. Cells (556) which could not be assigned as either CD4 or CD8 T cell based on
608 this criterion, were further assigned as $CD4^+$ (274) and $CD8^+$ (12) T cells if they shared the
609 clonotypes with an already assigned $CD4^+$ or $CD8^+$ T cell. Cells that could not be assigned to
610 either CD4 or CD8 category based on either of these criteria, were called as NA (not assigned)
611 cells (294). Based on these criteria, we had a total of 328 $CD4^+$ T cells, 536 $CD8^+$ T cells and
612 149 NA cells in cluster 2 (total 1013 cells) and 279 $CD4^+$ T cells, 199 $CD8^+$ T cells and 145
613 NA cells in cluster 4 (total 623 cells).

614 ***Statistical tests***

615 All the statistical tests were done using GraphPad Prism v9.0. Mann Whitney u-test was used
616 to perform pairwise comparison and *P*-value <0.05 was considered significant.

617 **Data and Code availability**

618 Scripts will be made available on GitHub (https://github.com/ImmunogenomicsLab-
619 NII/CMV-HD). Sequencing data for this study is deposited onto the Gene Expression Omnibus
620 with accession number GSE235604.

621

622 **References**

623 1. Kusnadi A, Ramirez-Suastegui C, Fajardo V, Chee SJ, Meckiff BJ, Simon H, Pelosi
624 E, Seumois G, Ay F, Vijayanand P, Ottensmeier CH: **Severely ill COVID-19**
625 **patients display impaired exhaustion features in SARS-CoV-2-reactive CD8(+) T**
626 **cells.** *Sci Immunol* 2021, **6**.

627 2. Lim EY, Jackson SE, Wills MR: **The CD4+ T Cell Response to Human**
628 **Cytomegalovirus in Healthy and Immunocompromised People.** *Front Cell Infect*
629 *Microbiol* 2020, **10:**202.

630 3. Meckiff BJ, Ramirez-Suastegui C, Fajardo V, Chee SJ, Kusnadi A, Simon H,
631 Eschweiler S, Grifoni A, Pelosi E, Weiskopf D, et al: **Imbalance of Regulatory and**
632 **Cytotoxic SARS-CoV-2-Reactive CD4(+) T Cells in COVID-19.** *Cell* 2020,
633 **183:**1340-1353 e1316.

634 4. Patil VS, Madrigal A, Schmiedel BJ, Clarke J, O'Rourke P, de Silva AD, Harris E,
635 Peters B, Seumois G, Weiskopf D, et al: **Precursors of human CD4(+) cytotoxic T**
636 **lymphocytes identified by single-cell transcriptome analysis.** *Sci Immunol* 2018, **3**.

637 5. Seumois G, Ramirez-Suastegui C, Schmiedel BJ, Liang S, Peters B, Sette A,
638 Vijayanand P: **Single-cell transcriptomic analysis of allergen-specific T cells in**
639 **allergy and asthma.** *Sci Immunol* 2020, **5**.

640 6. Lyu M, Wang S, Gao K, Wang L, Zhu X, Liu Y, Wang M, Liu X, Li B, Tian L:
641 **Dissecting the Landscape of Activated CMV-Stimulated CD4+ T Cells in**

642 **Humans by Linking Single-Cell RNA-Seq With T-Cell Receptor Sequencing.**
643 *Front Immunol* 2021, **12:**779961.
644 7. Lewis SA, Sutherland A, Soldevila F, Westernberg L, Aoki M, Frazier A, Maiche S,
645 Erlewyn-Lajeunesse M, Arshad H, Leonard S, et al: **Identification of cow milk**
646 **epitopes to characterize and quantify disease-specific T cells in allergic children.**
647 *J Allergy Clin Immunol* 2023.
648 8. O'Shea JJ, Paul WE: **Mechanisms underlying lineage commitment and plasticity**
649 **of helper CD4+ T cells.** *Science* 2010, **327:**1098-1102.
650 9. Schmiedel BJ, Singh D, Madrigal A, Valdovino-Gonzalez AG, White BM, Zapardiel-
651 Gonzalo J, Ha B, Altay G, Greenbaum JA, McVicker G, et al: **Impact of Genetic**
652 **Polymorphisms on Human Immune Cell Gene Expression.** *Cell* 2018, **175:**1701-
653 1715 e1716.
654 10. Arlehamn CL, Seumois G, Gerasimova A, Huang C, Fu Z, Yue X, Sette A,
655 Vijayanand P, Peters B: **Transcriptional profile of tuberculosis antigen-specific T**
656 **cells reveals novel multifunctional features.** *J Immunol* 2014, **193:**2931-2940.
657 11. Crotty S: **T Follicular Helper Cell Biology: A Decade of Discovery and Diseases.**
658 *Immunity* 2019, **50:**1132-1148.
659 12. Sallusto F: **Heterogeneity of Human CD4(+) T Cells Against Microbes.** *Annu Rev*
660 *Immunol* 2016, **34:**317-334.
661 13. Sakaguchi S, Sakaguchi N, Asano M, Itoh M, Toda M: **Immunologic self-tolerance**
662 **maintained by activated T cells expressing IL-2 receptor alpha-chains (CD25).**
663 **Breakdown of a single mechanism of self-tolerance causes various autoimmune**
664 **diseases.** *J Immunol* 1995, **155:**1151-1164.
665 14. Scheinecker C, Goschl L, Bonelli M: **Treg cells in health and autoimmune**
666 **diseases: New insights from single cell analysis.** *J Autoimmun* 2020, **110:**102376.

667 15. Mahnke YD, Brodie TM, Sallusto F, Roederer M, Lugli E: **The who's who of T-cell**
668 **differentiation: human memory T-cell subsets.** *Eur J Immunol* 2013, **43:**2797-
669 2809.
670 16. Jackson SE, Sedikides GX, Mason GM, Okecha G, Wills MR: **Human**
671 **Cytomegalovirus (HCMV)-Specific CD4(+) T Cells Are Polyfunctional and Can**
672 **Respond to HCMV-Infected Dendritic Cells In Vitro.** *J Virol* 2017, **91**.
673 17. van Leeuwen EM, Remmerswaal EB, Heemskerk MH, ten Berge IJ, van Lier RA:
674 **Strong selection of virus-specific cytotoxic CD4+ T-cell clones during primary**
675 **human cytomegalovirus infection.** *Blood* 2006, **108:**3121-3127.
676 18. van Leeuwen EM, Remmerswaal EB, Vossen MT, Rowshani AT, Wertheim-van
677 Dillen PM, van Lier RA, ten Berge IJ: **Emergence of a CD4+CD28- granzyme B+,**
678 **cytomegalovirus-specific T cell subset after recovery of primary cytomegalovirus**
679 **infection.** *J Immunol* 2004, **173:**1834-1841.
680 19. Gamadia LE, Rentenaar RJ, van Lier RA, ten Berge IJ: **Properties of CD4(+) T cells**
681 **in human cytomegalovirus infection.** *Hum Immunol* 2004, **65:**486-492.
682 20. Pachnio A, Ciaurriz M, Begum J, Lal N, Zuo J, Beggs A, Moss P: **Cytomegalovirus**
683 **Infection Leads to Development of High Frequencies of Cytotoxic Virus-Specific**
684 **CD4+ T Cells Targeted to Vascular Endothelium.** *PLoS Pathog* 2016,
685 **12:**e1005832.
686 21. Cheroutre H, Husain MM: **CD4 CTL: living up to the challenge.** *Semin Immunol*
687 2013, **25:**273-281.
688 22. Weiskopf D, Bangs DJ, Sidney J, Kolla RV, De Silva AD, de Silva AM, Crotty S,
689 Peters B, Sette A: **Dengue virus infection elicits highly polarized CX3CR1+**
690 **cytotoxic CD4+ T cells associated with protective immunity.** *Proc Natl Acad Sci U*
691 *S A* 2015, **112:**E4256-4263.

692 23. Gandhi MK, Khanna R: **Human cytomegalovirus: clinical aspects, immune**
693 **regulation, and emerging treatments.** *Lancet Infect Dis* 2004, **4:**725-738.
694 24. Tu W, Chen S, Sharp M, Dekker C, Manganello AM, Tongson EC, Maecker HT,
695 Holmes TH, Wang Z, Kemble G, et al: **Persistent and selective deficiency of CD4+**
696 **T cell immunity to cytomegalovirus in immunocompetent young children.** *J*
697 *Immunol* 2004, **172:**3260-3267.
698 25. Gratama JW, Brooimans RA, van der Holt B, Sintnicolaas K, van Doornum G,
699 Niesters HG, Lowenberg B, Cornelissen JJ: **Monitoring cytomegalovirus IE-1 and**
700 **pp65-specific CD4+ and CD8+ T-cell responses after allogeneic stem cell**
701 **transplantation may identify patients at risk for recurrent CMV reactivations.**
702 *Cytometry B Clin Cytom* 2008, **74:**211-220.
703 26. Einsele H, Roosnek E, Rufer N, Sinzger C, Riegler S, Loffler J, Grigoleit U, Moris A,
704 Rammensee HG, Kanz L, et al: **Infusion of cytomegalovirus (CMV)-specific T cells**
705 **for the treatment of CMV infection not responding to antiviral chemotherapy.**
706 *Blood* 2002, **99:**3916-3922.
707 27. Sester M, Sester U, Gartner B, Heine G, Girndt M, Mueller-Lantzsch N, Meyerhans
708 A, Kohler H: **Levels of virus-specific CD4 T cells correlate with cytomegalovirus**
709 **control and predict virus-induced disease after renal transplantation.**
710 *Transplantation* 2001, **71:**1287-1294.
711 28. Peggs KS, Verfuerth S, Pizzey A, Khan N, Guiver M, Moss PA, Mackinnon S:
712 **Adoptive cellular therapy for early cytomegalovirus infection after allogeneic**
713 **stem-cell transplantation with virus-specific T-cell lines.** *Lancet* 2003, **362:**1375-
714 1377.
715 29. Lilleri D, Fornara C, Chiesa A, Caldera D, Alessandrino EP, Gerna G: **Human**
716 **cytomegalovirus-specific CD4+ and CD8+ T-cell reconstitution in adult**

717 **allogeneic hematopoietic stem cell transplant recipients and immune control of**
718 **viral infection.** *Haematologica* 2008, **93:**248-256.
719 30. Gamadia LE, Remmerswaal EB, Weel JF, Bemelman F, van Lier RA, Ten Berge IJ:
720 **Primary immune responses to human CMV: a critical role for IFN-gamma-**
721 **producing CD4+ T cells in protection against CMV disease.** *Blood* 2003,
722 **101:**2686-2692.
723 31. Lilleri D, Fornara C, Revello MG, Gerna G: **Human cytomegalovirus-specific**
724 **memory CD8+ and CD4+ T cell differentiation after primary infection.** *J Infect*
725 *Dis* 2008, **198:**536-543.
726 32. Jackson SE, Mason GM, Wills MR: **Human cytomegalovirus immunity and**
727 **immune evasion.** *Virus Res* 2011, **157:**151-160.
728 33. Khan N, Cobbold M, Keenan R, Moss PA: **Comparative analysis of CD8+ T cell**
729 **responses against human cytomegalovirus proteins pp65 and immediate early 1**
730 **shows similarities in precursor frequency, oligoclonality, and phenotype.** *J Infect*
731 *Dis* 2002, **185:**1025-1034.
732 34. Sylwester AW, Mitchell BL, Edgar JB, Taormina C, Pelte C, Ruchti F, Sleath PR,
733 Grabstein KH, Hosken NA, Kern F, et al: **Broadly targeted human**
734 **cytomegalovirus-specific CD4+ and CD8+ T cells dominate the memory**
735 **compartments of exposed subjects.** *J Exp Med* 2005, **202:**673-685.
736 35. Jackson SE, Sedikides GX, Okecha G, Wills MR: **Generation, maintenance and**
737 **tissue distribution of T cell responses to human cytomegalovirus in lytic and**
738 **latent infection.** *Med Microbiol Immunol* 2019, **208:**375-389.
739 36. Terrazzini N, Bajwa M, Vita S, Cheek E, Thomas D, Seddiki N, Smith H, Kern F: **A**
740 **novel cytomegalovirus-induced regulatory-type T-cell subset increases in size**

741 **during older life and links virus-specific immunity to vascular pathology.** *J Infect*
742 *Dis* 2014, **209:**1382-1392.
743 37. Tovar-Salazar A, Patterson-Bartlett J, Jesser R, Weinberg A: **Regulatory function of**
744 **cytomegalovirus-specific CD4+CD27-CD28- T cells.** *Virology* 2010, **398:**158-167.
745 38. Schwele S, Fischer AM, Brestrich G, Wlodarski MW, Wagner L, Schmueck M,
746 Roemhild A, Thomas S, Hammer MH, Babel N, et al: **Cytomegalovirus-specific**
747 **regulatory and effector T cells share TCR clonality--possible relation to**
748 **repetitive CMV infections.** *Am J Transplant* 2012, **12:**669-681.
749 39. Clement M, Marsden M, Stacey MA, Abdul-Karim J, Gimeno Brias S, Costa Bento
750 D, Scurr MJ, Ghazal P, Weaver CT, Carlesso G, et al: **Cytomegalovirus-Specific IL-**
751 **10-Producing CD4+ T Cells Are Governed by Type-I IFN-Induced IL-27 and**
752 **Promote Virus Persistence.** *PLoS Pathog* 2016, **12:**e1006050.
753 40. Bacher P, Scheffold A: **Flow-cytometric analysis of rare antigen-specific T cells.**
754 *Cytometry A* 2013, **83:**692-701.
755 41. Bacher P, Schink C, Teutschbein J, Kniemeyer O, Assenmacher M, Brakhage AA,
756 Scheffold A: **Antigen-reactive T cell enrichment for direct, high-resolution**
757 **analysis of the human naive and memory Th cell repertoire.** *J Immunol* 2013,
758 **190:**3967-3976.
759 42. Poloni C, Schonhofer C, Ivison S, Levings MK, Steiner TS, Cook L: **T-cell**
760 **activation-induced marker assays in health and disease.** *Immunol Cell Biol* 2023.
761 43. Best JA, Blair DA, Knell J, Yang E, Mayya V, Doedens A, Dustin ML, Goldrath AW,
762 Immunological Genome Project C: **Transcriptional insights into the CD8(+) T cell**
763 **response to infection and memory T cell formation.** *Nat Immunol* 2013, **14:**404-
764 412.

765 44. Bahr F, Wehner R, Platzbecker U, Wermke M, Shayegi N, Middeke JM, Rollig C,
766 Schetelig J, Ehninger G, Schmitz M, et al: **Reconstitution of interleukin-17-**
767 **producing T helper cells after allogeneic hematopoietic cell transplantation.** *Biol*
768 *Blood Marrow Transplant* 2013, **19:**357-365.
769 45. Schober K, Voit F, Grassmann S, Muller TR, Eggert J, Jarosch S, Weissbrich B,
770 Hoffmann P, Borkner L, Nio E, et al: **Reverse TCR repertoire evolution toward**
771 **dominant low-affinity clones during chronic CMV infection.** *Nat Immunol* 2020,
772 **21:**434-441.
773 46. Klenerman P, Oxenius A: **T cell responses to cytomegalovirus.** *Nat Rev Immunol*
774 2016, **16:**367-377.
775 47. Seddiki N, Santner-Nanan B, Martinson J, Zaunders J, Sasson S, Landay A, Solomon
776 M, Selby W, Alexander SI, Nanan R, et al: **Expression of interleukin (IL)-2 and IL-**
777 **7 receptors discriminates between human regulatory and activated T cells.** *J Exp*
778 *Med* 2006, **203:**1693-1700.
779 48. Tovar-Salazar A, Weinberg A: **Understanding the mechanism of action of**
780 **cytomegalovirus-induced regulatory T cells.** *Virology* 2020, **547:**1-6.
781 49. Velaga S, Ukena SN, Hopting M, Ivanyi P, Borchers S, Mischak-Weissinger EM,
782 Hamwi I, Buchholz S, Ganser A, Franzke A: **Reconstitution and phenotype of**
783 **Tregs in CMV reactivating patients following allogeneic hematopoietic stem cell**
784 **transplantation.** *Immunol Invest* 2013, **42:**18-35.
785 50. Almanan M, Raynor J, Sholl A, Wang M, Chougnet C, Cardin RD, Hildeman DA:
786 **Tissue-specific control of latent CMV reactivation by regulatory T cells.** *PLoS*
787 *Pathog* 2017, **13:**e1006507.
788 51. Miyara M, Yoshioka Y, Kitoh A, Shima T, Wing K, Niwa A, Parizot C, Taflin C,
789 Heike T, Valeyre D, et al: **Functional delineation and differentiation dynamics of**

790 **human CD4+ T cells expressing the FoxP3 transcription factor.** *Immunity* 2009,
791 **30:**899-911.
792 52. Valmori D, Raffin C, Raimbaud I, Ayyoub M: **Human RORgammat+ TH17 cells**
793 **preferentially differentiate from naive FOXP3+Treg in the presence of lineage-**
794 **specific polarizing factors.** *Proc Natl Acad Sci U S A* 2010, **107:**19402-19407.
795 53. Matsuki F, Saegusa J, Miyamoto Y, Misaki K, Kumagai S, Morinobu A: **CD45RA-**
796 **Foxp3(high) activated/effector regulatory T cells in the CCR7 + CD45RA-CD27**
797 **+ CD28+central memory subset are decreased in peripheral blood from patients**
798 **with rheumatoid arthritis.** *Biochem Biophys Res Commun* 2013, **438:**778-783.
799 54. Nowak A, Lock D, Bacher P, Hohnstein T, Vogt K, Gottfreund J, Giehr P, Polansky
800 JK, Sawitzki B, Kaiser A, et al: **CD137+CD154- Expression As a Regulatory T**
801 **Cell (Treg)-Specific Activation Signature for Identification and Sorting of Stable**
802 **Human Tregs from In Vitro Expansion Cultures.** *Front Immunol* 2018, **9:**199.
803 55. Jayaratne HE, Wijeratne D, Fernando S, Kamaladasa A, Gomes L, Wijewickrama A,
804 Ogg GS, Malavige GN: **Regulatory T-cells in acute dengue viral infection.**
805 *Immunology* 2018, **154:**89-97.
806 56. Deaglio S, Dwyer KM, Gao W, Friedman D, Usheva A, Erat A, Chen JF, Enjyoji K,
807 Linden J, Oukka M, et al: **Adenosine generation catalyzed by CD39 and CD73**
808 **expressed on regulatory T cells mediates immune suppression.** *J Exp Med* 2007,
809 **204:**1257-1265.
810 57. Raffin C, Pignon P, Celse C, Debien E, Valmori D, Ayyoub M: **Human memory**
811 **Helios- FOXP3+ regulatory T cells (Tregs) encompass induced Tregs that**
812 **express Aiolos and respond to IL-1beta by downregulating their suppressor**
813 **functions.** *J Immunol* 2013, **191:**4619-4627.

814 58. Shevach EM: **Mechanisms of foxp3+ T regulatory cell-mediated suppression.**
815 *Immunity* 2009, **30:**636-645.
816 59. Sefik E, Geva-Zatorsky N, Oh S, Konnikova L, Zemmour D, McGuire AM, Burzyn
817 D, Ortiz-Lopez A, Lobera M, Yang J, et al: **MUCOSAL IMMUNOLOGY.**
818 **Individual intestinal symbionts induce a distinct population of RORgamma(+)**
819 **regulatory T cells.** *Science* 2015, **349:**993-997.
820 60. Koch MA, Tucker-Heard G, Perdue NR, Killebrew JR, Urdahl KB, Campbell DJ:
821 **The transcription factor T-bet controls regulatory T cell homeostasis and**
822 **function during type 1 inflammation.** *Nat Immunol* 2009, **10:**595-602.
823 61. Wang Y, Su MA, Wan YY: **An essential role of the transcription factor GATA-3**
824 **for the function of regulatory T cells.** *Immunity* 2011, **35:**337-348.
825 62. Zheng Y, Chaudhry A, Kas A, deRoos P, Kim JM, Chu TT, Corcoran L, Treuting P,
826 Klein U, Rudensky AY: **Regulatory T-cell suppressor program co-opts**
827 **transcription factor IRF4 to control T(H)2 responses.** *Nature* 2009, **458:**351-356.
828 63. Chu Y, Dai E, Li Y, Han G, Pei G, Ingram DR, Thakkar K, Qin JJ, Dang M, Le X, et
829 al: **Pan-cancer T cell atlas links a cellular stress response state to immunotherapy**
830 **resistance.** *Nat Med* 2023.
831 64. Eschweiler S, Clarke J, Ramirez-Suastegui C, Panwar B, Madrigal A, Chee SJ,
832 Karydis I, Woo E, Alzetani A, Elsheikh S, et al: **Intratumoral follicular regulatory**
833 **T cells curtail anti-PD-1 treatment efficacy.** *Nat Immunol* 2021, **22:**1052-1063.
834 65. Xie MM, Fang S, Chen Q, Liu H, Wan J, Dent AL: **Follicular regulatory T cells**
835 **inhibit the development of granzyme B-expressing follicular helper T cells.** *JCI*
836 *Insight* 2019, **4**.

837 66. Wagner L, Yang OO, Garcia-Zepeda EA, Ge Y, Kalams SA, Walker BD, Pasternack
838 MS, Luster AD: **Beta-chemokines are released from HIV-1-specific cytolytic T-**
839 **cell granules complexed to proteoglycans.** *Nature* 1998, **391:**908-911.
840 67. Caccamo N, Milano S, Di Sano C, Cigna D, Ivanyi J, Krensky AM, Dieli F, Salerno
841 A: **Identification of epitopes of Mycobacterium tuberculosis 16-kDa protein**
842 **recognized by human leukocyte antigen-A*0201 CD8(+) T lymphocytes.** *J Infect*
843 *Dis* 2002, **186:**991-998.
844 68. Eberlein J, Davenport B, Nguyen TT, Victorino F, Jhun K, van der Heide V,
845 Kuleshov M, Ma'ayan A, Kedl R, Homann D: **Chemokine Signatures of Pathogen-**
846 **Specific T Cells I: Effector T Cells.** *J Immunol* 2020, **205:**2169-2187.
847 69. Awwad MHS, Mahmoud A, Bruns H, Echchannaoui H, Kriegsmann K, Lutz R, Raab
848 MS, Bertsch U, Munder M, Jauch A, et al: **Selective elimination of**
849 **immunosuppressive T cells in patients with multiple myeloma.** *Leukemia* 2021,
850 **35:**2602-2615.
851 70. Sumida H, Cyster JG: **G-Protein Coupled Receptor 18 Contributes to**
852 **Establishment of the CD8 Effector T Cell Compartment.** *Front Immunol* 2018,
853 **9:**660.
854 71. Correa-Rocha R, Lopez-Abente J, Gutierrez C, Perez-Fernandez VA, Prieto-Sanchez
855 A, Moreno-Guillen S, Munoz-Fernandez MA, Pion M: **CD72/CD100 and PD-1/PD-**
856 **L1 markers are increased on T and B cells in HIV-1+ viremic individuals, and**
857 **CD72/CD100 axis is correlated with T-cell exhaustion.** *PLoS One* 2018,
858 **13:**e0203419.
859 72. Omilusik KD, Best JA, Yu B, Goossens S, Weidemann A, Nguyen JV, Seuntjens E,
860 Stryjewska A, Zweier C, Roychoudhuri R, et al: **Transcriptional repressor ZEB2**

861 **promotes terminal differentiation of CD8+ effector and memory T cell**
862 **populations during infection.** *J Exp Med* 2015, **212:**2027-2039.
863 73. Zhang L, Zhou R, Zhang W, Yao X, Li W, Xu L, Sun X, Zhao L: **Cysteine-rich**
864 **intestinal protein 1 suppresses apoptosis and chemosensitivity to 5-fluorouracil**
865 **in colorectal cancer through ubiquitin-mediated Fas degradation.** *J Exp Clin*
866 *Cancer Res* 2019, **38:**120.
867 74. Chaudhuri L, Srivastava RK, Kos F, Shrikant PA: **Uncoupling protein 2 regulates**
868 **metabolic reprogramming and fate of antigen-stimulated CD8+ T cells.** *Cancer*
869 *Immunol Immunother* 2016, **65:**869-874.
870 75. Stegelmann F, Bastian M, Swoboda K, Bhat R, Kiessler V, Krensky AM,
871 Roellinghoff M, Modlin RL, Stenger S: **Coordinate expression of CC chemokine**
872 **ligand 5, granulysin, and perforin in CD8+ T cells provides a host defense**
873 **mechanism against Mycobacterium tuberculosis.** *J Immunol* 2005, **175:**7474-7483.
874 76. Pena SV, Hanson DA, Carr BA, Goralski TJ, Krensky AM: **Processing, subcellular**
875 **localization, and function of 519 (granulysin), a human late T cell activation**
876 **molecule with homology to small, lytic, granule proteins.** *J Immunol* 1997,
877 **158:**2680-2688.
878 77. Pena SV, Krensky AM: **Granulysin, a new human cytolytic granule-associated**
879 **protein with possible involvement in cell-mediated cytotoxicity.** *Semin Immunol*
880 1997, **9:**117-125.
881 78. Gubser PM, Bantug GR, Razik L, Fischer M, Dimeloe S, Hoenger G, Durovic B,
882 Jauch A, Hess C: **Rapid effector function of memory CD8+ T cells requires an**
883 **immediate-early glycolytic switch.** *Nat Immunol* 2013, **14:**1064-1072.

884 79. Rangel Rivera GO, Knochelmann HM, Dwyer CJ, Smith AS, Wyatt MM, Rivera-
885 Reyes AM, Thaxton JE, Paulos CM: **Fundamentals of T Cell Metabolism and**
886 **Strategies to Enhance Cancer Immunotherapy.** *Front Immunol* 2021, **12:**645242.
887 80. Cham CM, Gajewski TF: **Glucose availability regulates IFN-gamma production**
888 **and p70S6 kinase activation in CD8+ effector T cells.** *J Immunol* 2005, **174:**4670-
889 4677.
890 81. Hao Y, Hao S, Andersen-Nissen E, Mauck WM, 3rd, Zheng S, Butler A, Lee MJ,
891 Wilk AJ, Darby C, Zager M, et al: **Integrated analysis of multimodal single-cell**
892 **data.** *Cell* 2021, **184:**3573-3587 e3529.
893 82. Stoeckius M, Zheng S, Houck-Loomis B, Hao S, Yeung BZ, Mauck WM, 3rd,
894 Smibert P, Satija R: **Cell Hashing with barcoded antibodies enables multiplexing**
895 **and doublet detection for single cell genomics.** *Genome Biol* 2018, **19:**224.
896 83. Subramanian A, Tamayo P, Mootha VK, Mukherjee S, Ebert BL, Gillette MA,
897 Paulovich A, Pomeroy SL, Golub TR, Lander ES, Mesirov JP: **Gene set enrichment**
898 **analysis: a knowledge-based approach for interpreting genome-wide expression**
899 **profiles.** *Proc Natl Acad Sci U S A* 2005, **102:**15545-15550.
900 84. Street K, Risso D, Fletcher RB, Das D, Ngai J, Yosef N, Purdom E, Dudoit S:
901 **Slingshot: cell lineage and pseudotime inference for single-cell transcriptomics.**
902 *BMC Genomics* 2018, **19:**477.

903

904 **Acknowledgements**

905 We thank the members of Immunogenomics laboratory at National Institute of Immunology
906 (NII) for useful discussions and suggestions.

907 **Funding**

908 This work was supported by the DBT/Wellcome Trust India Alliance Fellowship (grant
909 number IA/I/18/2/504012) awarded to VSP and DBT-NII core funding to VSP. RK is
910 supported by DBT-JRF (Department of Biotechnology-Junior Research Fellowship) for his
911 PhD.

912 **Author information**

913 Authors and Affiliation

914 National Institute of Immunology, Aruna Asaf Ali Marg, New Delhi, India
915 Raunak Kar, Somdeb Chattopadhyay, Kirti Sharma, Shreya Sinha, Gopalakrishnan
916 Aneeshkumar Arimbasseri, Veena S. Patil
917
918 Vardhman Mahavir Medical College and Safdarjung Hospital, New Delhi, India
919 Anjali Sharma
920
921 Corresponding authors
922 Correspondence to Gopalakrishnan Aneeshkumar Arimbasseri (aneesh@nii.ac.in) or Veena S.
923 Patil (veena@nii.ac.in)
924 Lead contact: Veena S. Patil (veena@nii.ac.in)
925

926 Contributions

927 RK and VSP conceived, designed, and executed the study. RK, KS and SS performed and
928 analysed the experiments under the supervision of VSP, Genomics data was analysed by RK
929 and SC under the supervision of GAA and VSP, AS supervised patient recruitment and sample
930 collection, RK and VSP wrote the manuscript, which was further edited and approved by all
931 authors.
932

933 **Ethics declaration**

934 Ethics approval and consent to participate

935 Approval for the use of human material for research was obtained from the institutional human
936 ethics committees from both National Institute of Immunology, New Delhi and Vardhman
937 Mahavir Medical College (VMMC) and Safdarjung Hospital, New Delhi, India. The donors
938 consented for use of the plasma and buffy coat samples for research.

939

940 **Competing interests**

941 The authors declare that they have no competing interests.

942

943 **Figure Legends**

944 **Fig. 1. Single-cell transcriptomic analysis of hCMV-reactive memory T cell subsets.** (A)
945 Schematic showing the study overview of isolating and single-cell RNA-seq of hCMV-specific
946 T cells using 10X Genomics platform. Histograms (on the right) shows cells isolated using
947 FACS for single-cell RNA-Seq from indicated T cell memory compartment from 10 donors.
948 (B) 2D UMAP of single-cell RNA-Seq data from 6899 cells, using 2000 most variable
949 transcripts, shows 9 distinct clusters of cells of hCMV-specific T cells. (C) 2D UMAP plots
950 (top) and violin plots (bottom) show expression of the indicated protein (oligo-tagged
951 antibodies; adt). Colour scale shows expression levels of individual cells (UMAP) or mean
952 expression in each cluster (violin plot). Only cells (6067) obtained from experiment 2 with 10
953 donors are shown. (D) Dot plots show the mean expression (colour) and percentage of
954 expressing cells (size) for selected marker gene transcripts in each cluster. (E) 2D UMAP plots
955 of single-cell RNA-Seq data show the expression of the *CD4*, *CD8A* and *CD8B* transcripts.
956 Scale represents expression level of the given transcript. Cells with zero counts for the indicated
957 transcript are shown in grey colour. (F) 2D UMAP plots show the T_{CM}, T_{EM} and T_{EMRA}

958 signature score for each cell. (G) 2D UMAP plots (left) of single-cell RNA-Seq data show the
959 expression of the *CD154* (top) and *CD137* (bottom) transcripts. Scale represents expression
960 level of the given transcript. Cells with zero counts for the indicated transcripts are shown in
961 grey colour. Scatter plots (right) show the co-expression matrix for *CD154* (on X-axis), and
962 *CD137* (on Y-axis) with *CD69* or *TNFRSF4* (colour scale: mean expression) transcripts. For
963 violin plots in (C) and dot plots in (D) cluster with less than 1% of the total cells is not shown
964 (cluster 8=56 cells). All expression counts for transcripts are $\log_2$ normalized (CPM+1).

965 **Fig. 2. hCMV-reactive T cell subtypes and their TCR clonal diversity.** (A) Heatmap shows
966 the expression of the most significantly enriched transcripts in each cluster. The top 200
967 transcripts are shown based on adjusted *P* value < 0.05, $\log_2$ fold change > 0.25 and > 10%
968 difference in the percentage of cells expressing selected transcript between two groups of cells
969 compared. Each column represents the average expression of all cells for a given cluster.
970 Colour scale represents z-score for the expression of each transcript across clusters. (B) Dot
971 plots show the mean expression (colour) and percentage of expressing cells (size) for selected
972 marker gene transcript in each cluster. (C) 2D UMAP plots show the IFN response, T_{REG},
973 cytotoxicity and cell cycle signature score for each cell. (D) Violin plots show the normalized
974 expression level ($\log_2$(CPM+1)) of the indicated differentially expressed transcript. Colour
975 scale shows percentage of cells expressing the indicated transcript for each cluster. (E) Bar
976 graph shows the percentage of cells with expanded clonotypes (frequency≥2) across 9 clusters.
977 (F) Bar graph shows the frequency of 25 most expanded clonotypes across different clusters.
978 For B and D, clusters with <1% of the total cells are not shown (cluster 8=56 cells).

979 **Fig. 3. Single-cell transcriptomic analysis of hCMV-reactive T_{REG}s.** (A) 2D UMAP plots
980 of single-cell RNA-Seq data show the expression of the *FOXP3*, *IL2RA*, *IKZF2* (left) and
981 joint expression of *FOXP3* with *IL2RA* and *FOXP3* with *IKZF2* (right 2 plots) transcripts.
982 Scale represents $\log_2$ normalized (CPM+1) counts for expression values and scaled density

983 for joint expression plots. Cells with zero counts for the indicated transcripts are shown in
984 grey colour. (B) Bar graph shows the percentage of cells expressing *FOXP3* transcript
985 (log_2(CPM+1)>0) in clusters 1 and 5. (C) Dot plots show the mean expression (colour) and
986 percentage of expressing cells (size) for selected marker gene transcripts in indicated clusters.
987 Clusters with <1% of the total cells are not shown (cluster 8=56 cells). (D) Scatter plots
988 showing normalized co-expression level (log2(CPM+1)) between *FOXP3* and *GATA3* and
989 *FOXP3* and *IL2RA* transcripts in the indicated clusters. (E) Bar graph shows the percentage
990 of cells expressing *GATA3* or *IL1R2* transcripts (log_2(CPM+1)>0) within *FOXP3* transcript
991 expressing cells in clusters 1 and 5. (F) 2D UMAP plots show joint expression of *FOXP3* +
992 *GATA3*, *FOXP3* + *CCR4* and *FOXP3* + *IL1R2*, *FOXP3* + *CCR8*. (G) Violin plot shows the
993 module enrichment score for T_H2-specific gene set across 8 clusters. Colour scale indicates
994 mean module score. Clusters with <1% of the total cells are not shown (cluster 8=56 cells).
995 (H) Gene set enrichment plot for T_H2 specific gene sets in cluster 1 and cluster 5 versus all
996 the other cluster. RES: Running Enrichment Score; NES: Normalized Enrichment Score;
997 FDR: False Discovery Rate. (I) 2D UMAP plot shows joint expression of T_H2-specific gene
998 set and allergy induced T_{REG}-specific gene set. Scale represents density for joint expression
999 plot.

1000 **Fig. 4. Single-cell transcriptomic analysis of hCMV-reactive CD4-CTLs and CD8-CTLs.**
1001 (A) 2D UMAP plots of single-cell RNA-Seq data show the expression of the indicated
1002 transcripts. All expression counts for transcripts are log_2 normalized (CPM+1). Cells with zero
1003 counts for the indicated transcripts are shown in grey colour. (B) Dot plots show the mean
1004 expression (colour) and percentage of expressing cells (size) for selected marker gene
1005 transcripts in each cluster. (C) Violin plots showing the normalized expression level
1006 (log_2(CPM+1)) of the indicated differentially expressed transcripts across 8 clusters. Colour
1007 scale shows percentage of cells expressing the indicated transcript for a given cluster. (D)

1008 Trajectory analysis using slingshot shows the distribution of cells from indicated clusters
1009 (middle) on a pseudo-scale (left), and expression levels (scale) of the *GZMB*, *GNLY*, *CRTAM*
1010 and *KLRD1* transcripts. (E) 2D UMAP plot shows the cells with same clonotypes (colours)
1011 shared between cluster 3 and, clusters 2 and 4. (F) Pie chart shows the distribution of percentage
1012 of cells expressing the top 20 expanded clonotypes in clusters 2 and 4. (G) Stacked bar graph
1013 shows the proportion of CD4, CD8 and NA (not assigned) T cells in each indicated cluster
1014 (refer to methods section for classification of cells). (H) Heatmap shows the normalized
1015 expression of 50 differentially expressed transcripts from each clusters 2 and 4 when compared
1016 to the rest of the clusters. (I) Violin plots show the normalized expression level ($\log_2$(CPM+1))
1017 of the indicated differentially expressed transcript across indicated T cell subsets in clusters 2
1018 and 4. Colour scale shows percentage of cells expressing the indicated transcript. For B and C,
1019 clusters with <1% of the total cells are not shown (cluster 8=56 cells).

1020

1021 **Additional files**

1022 **Additional file 1. Supplementary figures.**

1023 **Fig. S1. Single-cell RNA-Seq of hCMV-specific cells.** (A) Graph shows the hCMV-specific
1024 IgG positivity (normalized absorbance) in 126 human donors. (B) Contour plots showing the
1025 gating strategy used to analyse the activated T cells in the indicated subsets upon stimulation
1026 of the PBMCs with hCMV peptide pools. (C) Violin plot shows the normalized T cell reactivity
1027 to hCMV-specific peptide pools compared to unstimulated control. Donors above the
1028 horizontal dotted line for memory compartments were chosen for further single-cell genomics
1029 studies (10 out of 16). (C) Stacked bar graph shows the distribution of cells from different
1030 donors across 9 clusters. (D) Stacked bar graph (left) and the 2D UMAPs (right) show the
1031 distribution of cells across 9 clusters from 2 different experiments/batch. Experiment 1

1032 included 3 donors (D1, D2 and D7) and experiment 2 included all 10 donors. (E) Violin plots
1033 show the module enrichment score for T_{CM}, T_{EM}, T_{EMRA}, T_{CM}-T_{EM}, and T_{EM} -T_{EMRA} specific
1034 gene sets across 8 clusters. Colour scale indicates average module score. Clusters with <1% of
1035 the total cells are not shown (cluster 8=56 cells).

1036 **Fig. S2. Functional characterization and TCR analysis of hCMV-specific T cells.** (A)
1037 Violin plots show the module enrichment score for T_H1, T_H17, and $T_H1/17$ subset-specific gene
1038 sets across 8 clusters. Colour scale indicates average module score. Clusters with <1% of the
1039 total cells are not shown (cluster 8=56 cells). (B) UpSet plot shows the TCR clonotypes
1040 (frequency on y-axis) and sharing of the clonotypes (bottom, connected dots) across the 9
1041 clusters. (C) Alluvial plot shows the clonally expanded cells (1234 cells) and their distribution
1042 and sharing across different clusters. Each connecting line represents a single cell.

1043 **Fig. S3. Pathways enriched in hCMV-specific cytotoxic clusters.** (A) Pathway enrichment
1044 analysis using Ingenuity Pathway Analysis (IPA) (Qiagen) shows enrichment of pathways in
1045 cluster 2 compared to cluster 4. (B) Pathway enrichment analysis using IPA shows enrichment
1046 of pathways in cluster 4 compared to cluster 2.

1047

1048 **Additional file 2: Supplementary Tables**

1049 **Table S1**. Details of cells from single-cell genomics experiments.

1050 **Table S2**: Details of reagents used in the study

1051 **Table S3**: Gene list used for enrichment analysis in the study

1052 **Table S4**. Single-cell cluster wise enrichment of transcripts using MAST (log2FC>0.25; adj
1053 pval <0.05)

1054 **Table S5**: TCR clonotype details of hCMV-reactive single-cells

Fig. 1

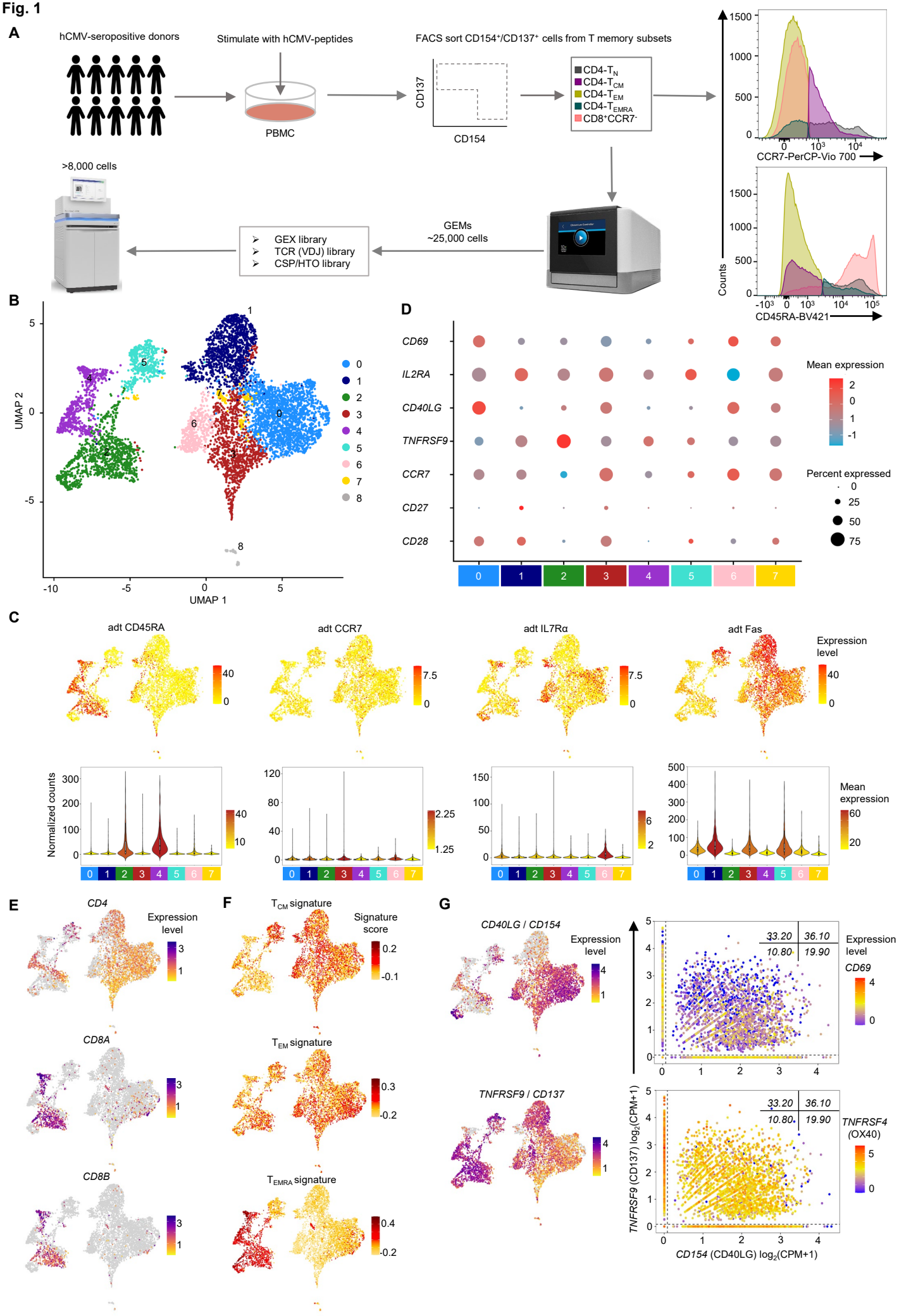
A
hCMV-seropositive donors
Stimulate with hCMV-peptides
PBMC
FACS sort CD154+/CD137+ cells from T memory subsets
CD137
CD154
CD4-TN
CD4-TCM
CD4-TEM
CD4-TEMRA
CD8+CCR7-
CCR7-PerCP-Vio 700
CD45RA-BV421
Counts
>8,000 cells
GEX library
TCR (VDJ) library
CSP/HTO library
GEMs
~25,000 cells
B
UMAP 1
UMAP 2
D
CD69
IL2RA
CD40LG
TNFRSF9
CCR7
CD27
CD28
Mean expression
Percent expressed
C
adt CD45RA
adt CCR7
adt IL7Rα
adt Fas
Expression level
Normalized counts
Mean expression
E
CD4
CD8A
CD8B
Expression level
F
TCM signature
TEM signature
TEMRA signature
Signature score
G
CD40LG / CD154
TNFRSF9 / CD137
Expression level
CD69
TNFRSF4 (OX40)
CD154 (CD40LG) log2(CPM+1)
TNFRSF9 (CD137) log2(CPM+1)

Fig. 2

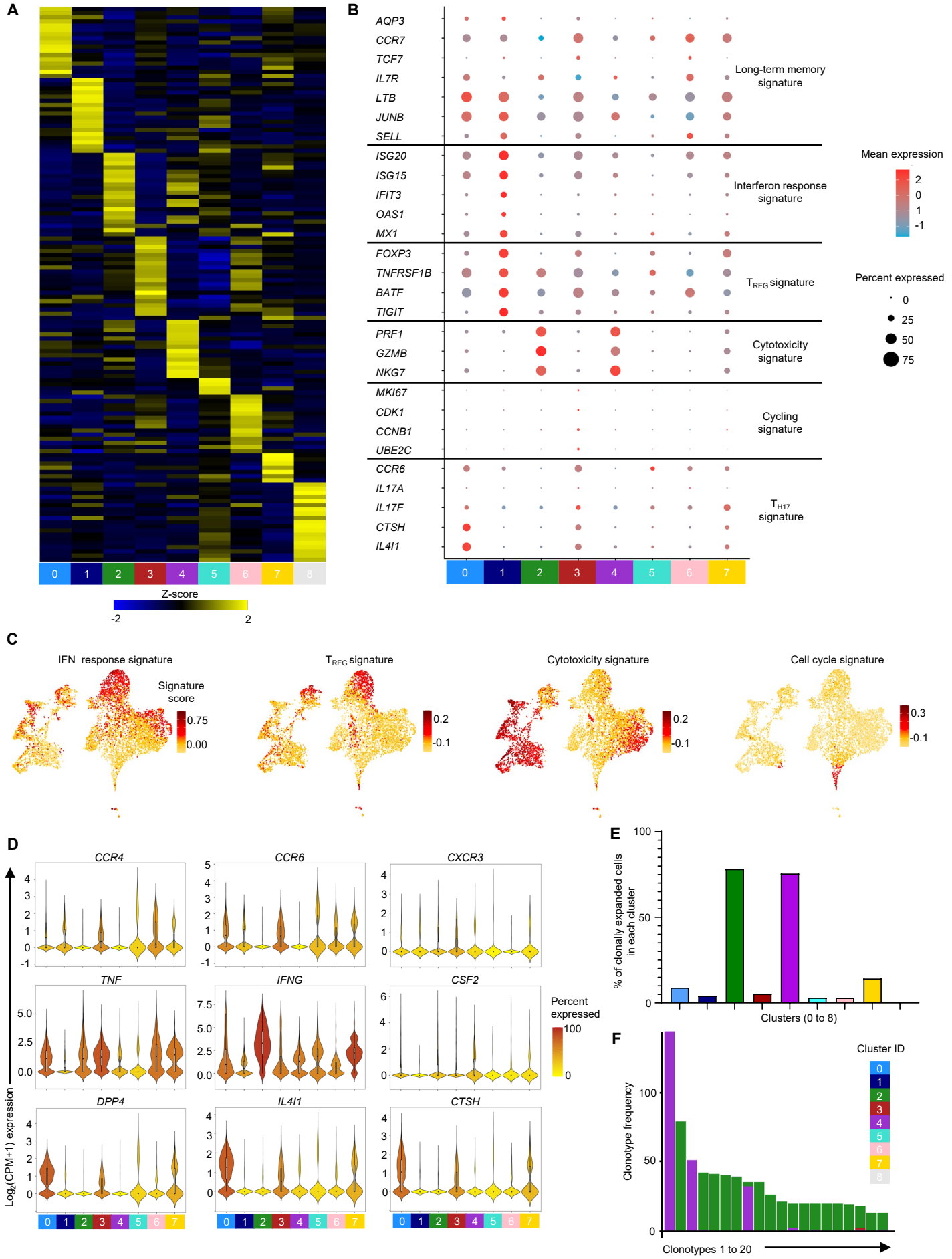
A
0 1 2 3 4 5 6 7 8
Z-score
-2
2
B
AQP3
CCR7
TCF7
IL7R
LTB
JUNB
SELL
Long-term memory signature
ISG20
ISG15
IFIT3
OAS1
MX1
Interferon response signature
FOXP3
TNFRSF1B
BATF
TIGIT
T_REG signature
PRF1
GZMB
NKG7
Cytotoxicity signature
MKI67
CDK1
CCNB1
UBE2C
Cycling signature
CCR6
IL17A
IL17F
CTSH
IL4I1
T_H17 signature
0 1 2 3 4 5 6 7
Mean expression
2
0
1
-1
Percent expressed
0
25
50
75
C
IFN response signature
Signature score
0.75
0.00
T_REG signature
0.2
-0.1
Cytotoxicity signature
0.2
-0.1
Cell cycle signature
0.3
-0.1
D
CCR4
CCR6
CXCR3
TNF
IFNG
CSF2
DPP4
IL4I1
CTSH
Log2(CPM+1) expression
Percent expressed
100
0
0 1 2 3 4 5 6 7
E
% of clonally expanded cells in each cluster
100
50
0
Clusters (0 to 8)
F
Clonotype frequency
100
50
0
Clonotypes 1 to 20
Cluster ID
0
1
2
3
4
5
6
7
8

Fig. 3

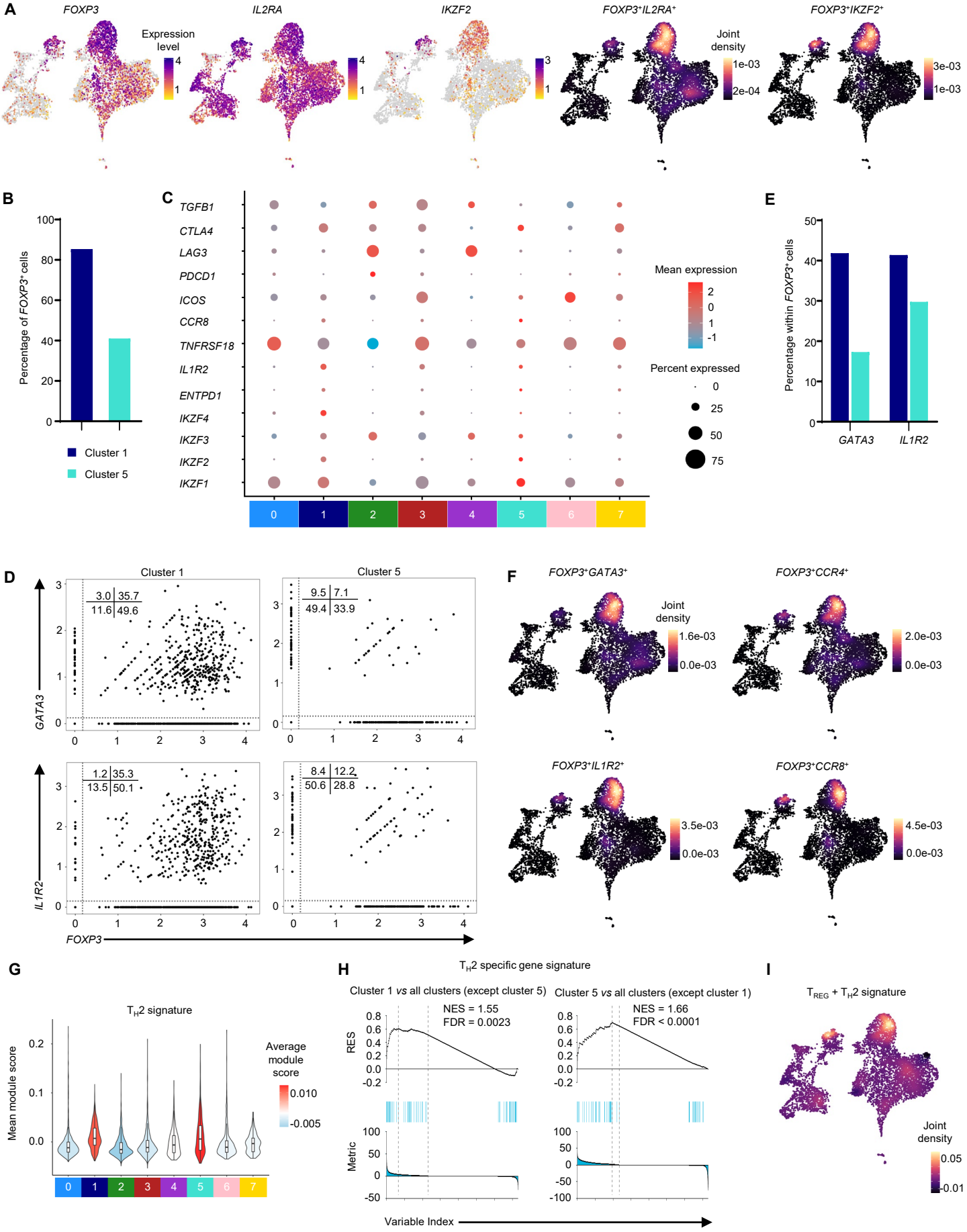
A
FOXP3
IL2RA
IKZF2
FOXP3+IL2RA+
FOXP3+IKZF2+
Expression level
Joint density
B
Percentage of FOXP3+ cells
Cluster 1
Cluster 5
C
TGFB1
CTLA4
LAG3
PDCD1
ICOS
CCR8
TNFRSF18
IL1R2
ENTPD1
IKZF4
IKZF3
IKZF2
IKZF1
Mean expression
Percent expressed
E
Percentage within FOXP3+ cells
GATA3
IL1R2
D
Cluster 1
Cluster 5
GATA3
IL1R2
FOXP3
F
FOXP3+GATA3+
FOXP3+CCR4+
FOXP3+IL1R2+
FOXP3+CCR8+
G
TH2 signature
Mean module score
Average module score
H
TH2 specific gene signature
Cluster 1 vs all clusters (except cluster 5)
Cluster 5 vs all clusters (except cluster 1)
NES = 1.55
FDR = 0.0023
NES = 1.66
FDR < 0.0001
RES
Metric
Variable Index
I
TREG + TH2 signature
Joint density

Fig. 4

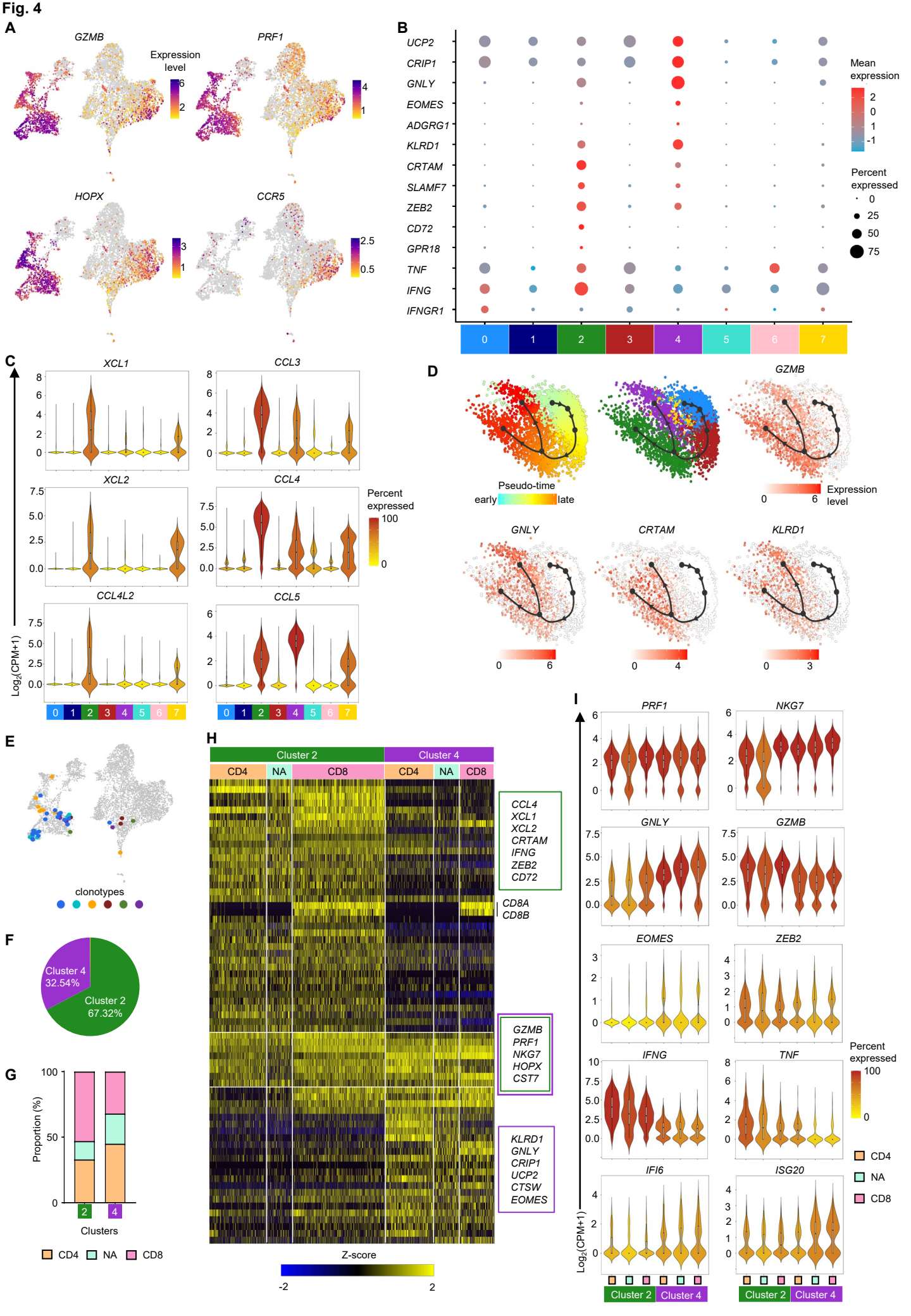
A
GZMB
PRF1
HOPX
CCR5
Expression level
B
UCP2
CRIP1
GNLY
EOMES
ADGRG1
KLRD1
CRTAM
SLAMF7
ZEB2
CD72
GPR18
TNF
IFNG
IFNGR1
Mean expression
Percent expressed
C
XCL1
CCL3
XCL2
CCL4
CCL4L2
CCL5
Percent expressed
Log2(CPM+1)
D
Pseudo-time
early
late
GZMB
Expression level
GNLY
CRTAM
KLRD1
E
clonotypes
F
Cluster 4 32.54%
Cluster 2 67.32%
G
Proportion (%)
Clusters
CD4
NA
CD8
H
Cluster 2
Cluster 4
CD4
NA
CD8
CCL4
XCL1
XCL2
CRTAM
IFNG
ZEB2
CD72
CD8A
CD8B
GZMB
PRF1
NKG7
HOPX
CST7
KLRD1
GNLY
CRIP1
UCP2
CTSW
EOMES
Z-score
I
PRF1
NKG7
GNLY
GZMB
EOMES
ZEB2
IFNG
TNF
IFI6
ISG20
Percent expressed
Log2(CPM+1)
Cluster 2
Cluster 4

Fig. S1

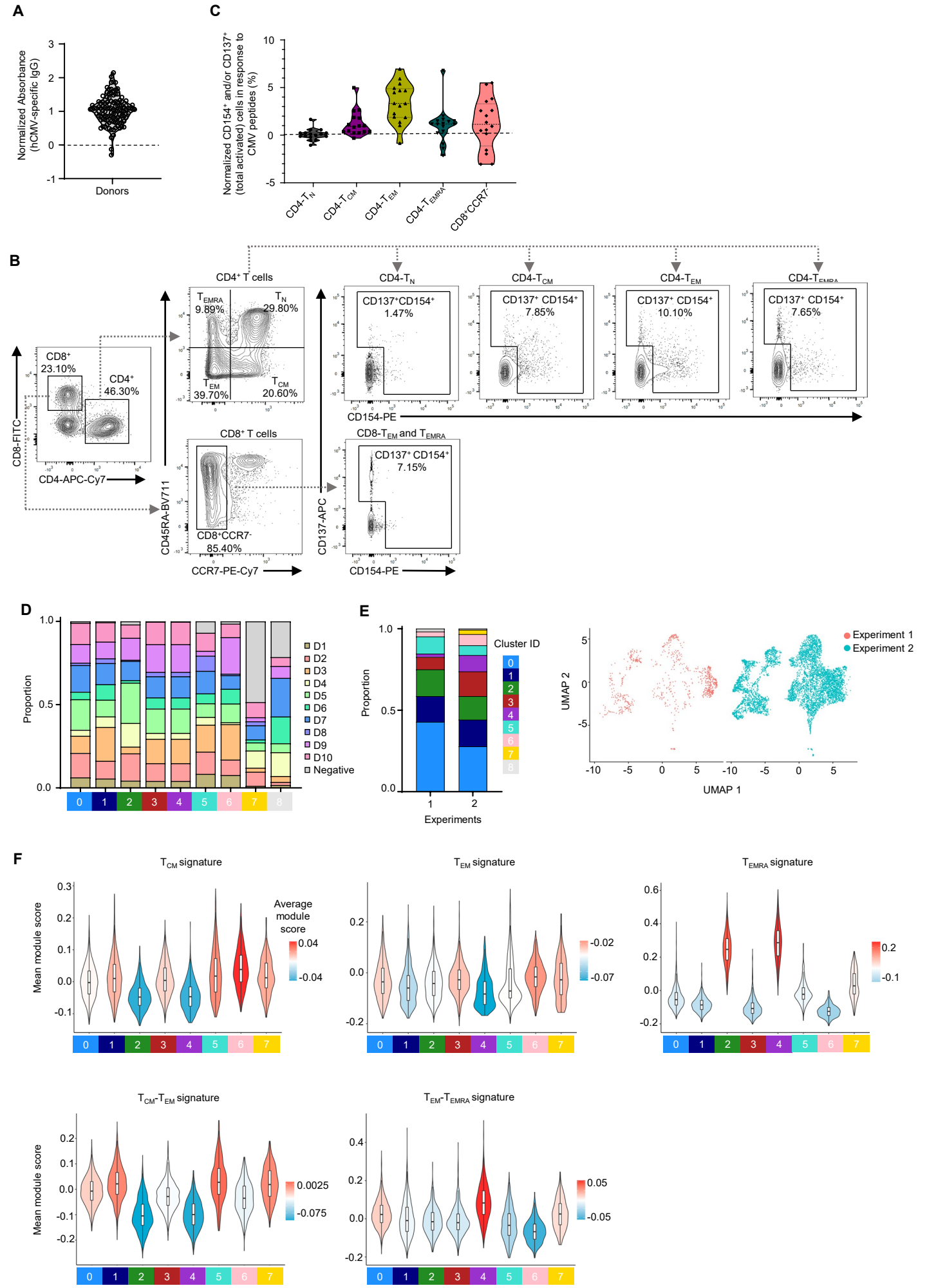
A
Normalized Absorbance (hCMV-specific IgG)
Donors
C
Normalized CD154+ and/or CD137+ (total activated) cells in response to CMV peptides (%)
CD4-TN
CD4-TCM
CD4-TEM
CD4-TEMRA
CD8+CCR7-
B
CD4+ T cells
CD8+ 23.10%
CD4+ 46.30%
CD8-FITC
CD4-APC-Cy7
TEMRA 9.89%
TN 29.80%
TEM 39.70%
TCM 20.60%
CD45RA-BV711
CD8+ T cells
CD8+CCR7- 85.40%
CCR7-PE-Cy7
CD4-TN
CD137+CD154+ 1.47%
CD4-TCM
CD137+ CD154+ 7.85%
CD4-TEM
CD137+ CD154+ 10.10%
CD4-TEMRA
CD137+ CD154+ 7.65%
CD154-PE
CD8-TEM and TEMRA
CD137+ CD154+ 7.15%
CD137-APC
CD154-PE
D
Proportion
D1
D2
D3
D4
D5
D6
D7
D8
D9
D10
Negative
E
Proportion
Cluster ID
Experiments
UMAP 2
UMAP 1
Experiment 1
Experiment 2
F
TCM signature
Mean module score
Average module score
TEM signature
TEMRA signature
TCM-TEM signature
TEM-TEMRA signature

Fig. S2

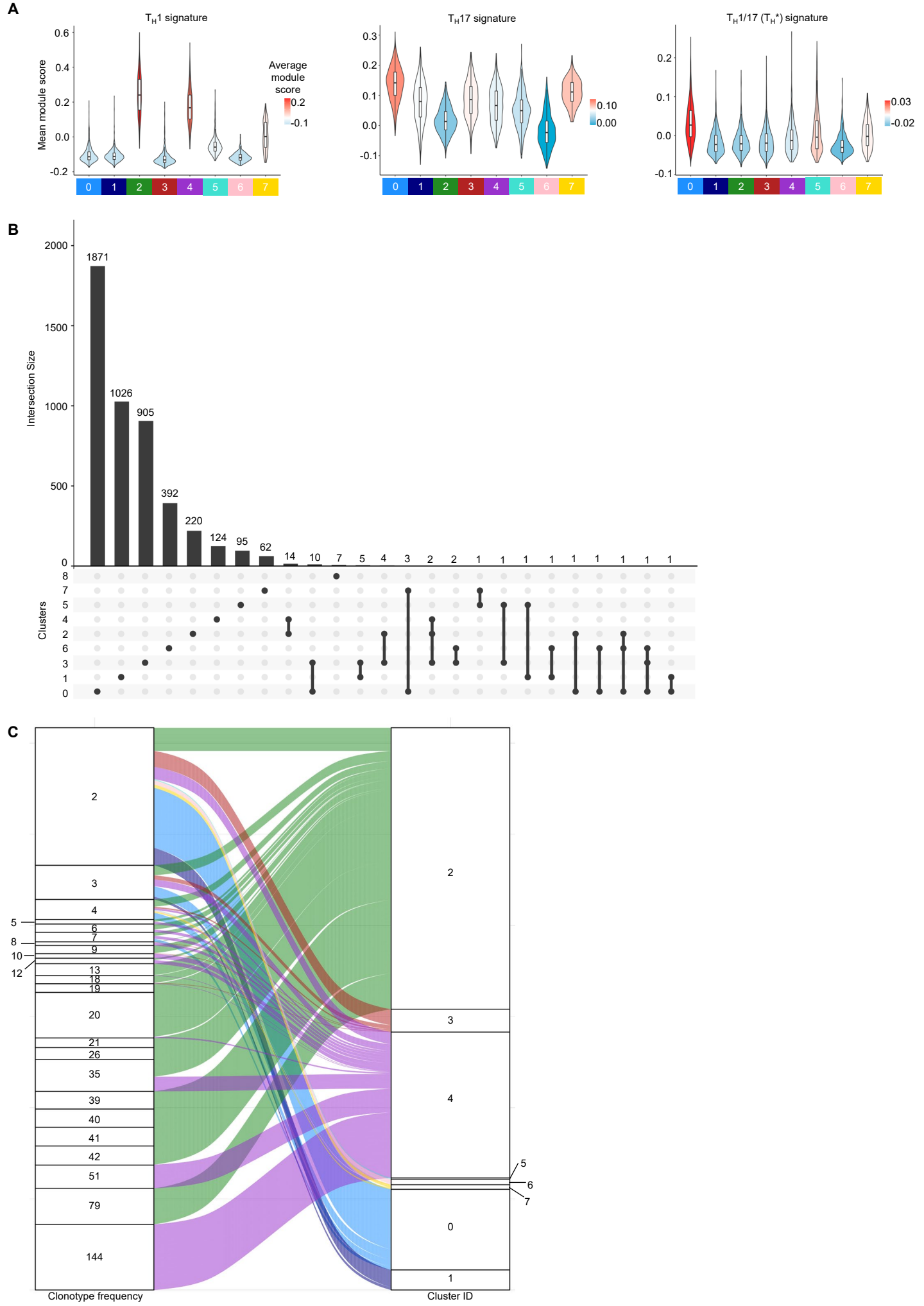
A
T_H1 signature
T_H17 signature
$T_H1/17$ (T_H*) signature
Mean module score
Average module score
0.2
-0.1
0.10
0.00
0.03
-0.02
0 1 2 3 4 5 6 7
B
Intersection Size
Clusters
1871
1026
905
392
220
124
95
62
14
10
7
5
4
3
2
2
1
1
1
1
1
1
1
1
1
C
Clonotype frequency
Cluster ID
2
3
4
5
6
7
8
9
10
12
13
18
19
20
21
26
35
39
40
41
42
51
79
144
2
3
4
5
6
7
0
1

Fig. S3

A

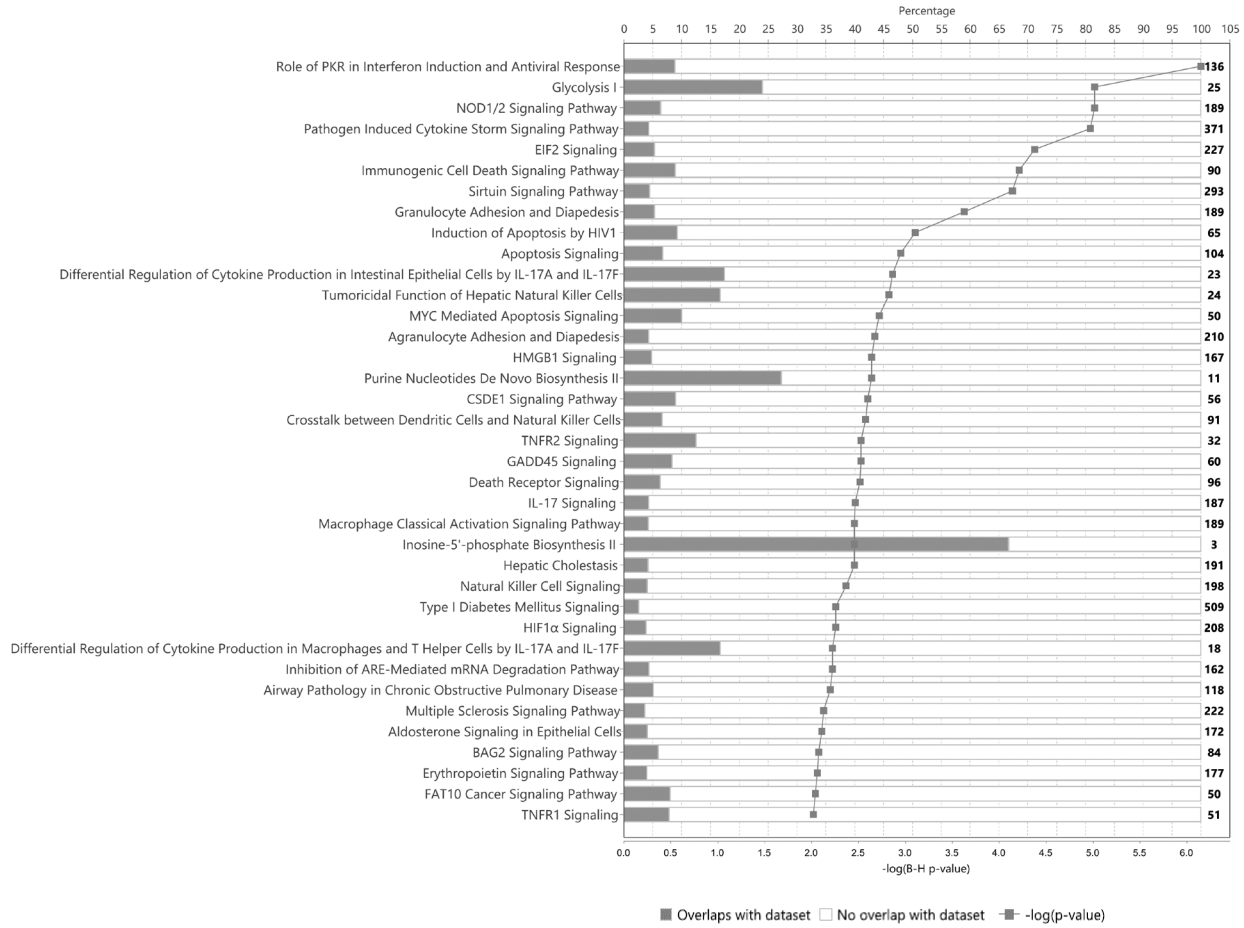
Percentage
0 5 10 15 20 25 30 35 40 45 50 55 60 65 70 75 80 85 90 95 100 105
Role of PKR in Interferon Induction and Antiviral Response 136
Glycolysis I 25
NOD1/2 Signaling Pathway 189
Pathogen Induced Cytokine Storm Signaling Pathway 371
EIF2 Signaling 227
Immunogenic Cell Death Signaling Pathway 90
Sirtuin Signaling Pathway 293
Granulocyte Adhesion and Diapedesis 189
Induction of Apoptosis by HIV1 65
Apoptosis Signaling 104
Differential Regulation of Cytokine Production in Intestinal Epithelial Cells by IL-17A and IL-17F 23
Tumoricidal Function of Hepatic Natural Killer Cells 24
MYC Mediated Apoptosis Signaling 50
Agranulocyte Adhesion and Diapedesis 210
HMGB1 Signaling 167
Purine Nucleotides De Novo Biosynthesis II 11
CSDE1 Signaling Pathway 56
Crosstalk between Dendritic Cells and Natural Killer Cells 91
TNFR2 Signaling 32
GADD45 Signaling 60
Death Receptor Signaling 96
IL-17 Signaling 187
Macrophage Classical Activation Signaling Pathway 189
Inosine-5'-phosphate Biosynthesis II 3
Hepatic Cholestasis 191
Natural Killer Cell Signaling 198
Type I Diabetes Mellitus Signaling 509
HIF1α Signaling 208
Differential Regulation of Cytokine Production in Macrophages and T Helper Cells by IL-17A and IL-17F 18
Inhibition of ARE-Mediated mRNA Degradation Pathway 162
Airway Pathology in Chronic Obstructive Pulmonary Disease 118
Multiple Sclerosis Signaling Pathway 222
Aldosterone Signaling in Epithelial Cells 172
BAG2 Signaling Pathway 84
Erythropoietin Signaling Pathway 177
FAT10 Cancer Signaling Pathway 50
TNFR1 Signaling 51
0.0 0.5 1.0 1.5 2.0 2.5 3.0 3.5 4.0 4.5 5.0 5.5 6.0
-log(B-H p-value)
Overlaps with dataset
No overlap with dataset
-log(p-value)

B

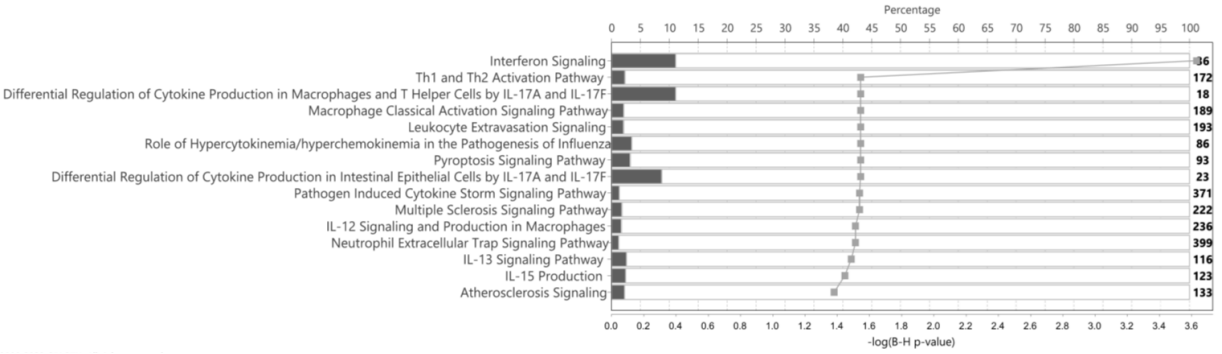
Percentage
0 5 10 15 20 25 30 35 40 45 50 55 60 65 70 75 80 85 90 95 100
Interferon Signaling 36
Th1 and Th2 Activation Pathway 172
Differential Regulation of Cytokine Production in Macrophages and T Helper Cells by IL-17A and IL-17F 18
Macrophage Classical Activation Signaling Pathway 189
Leukocyte Extravasation Signaling 193
Role of Hypercytokinemia/hyperchemokinemia in the Pathogenesis of Influenza 86
Pyroptosis Signaling Pathway 93
Differential Regulation of Cytokine Production in Intestinal Epithelial Cells by IL-17A and IL-17F 23
Pathogen Induced Cytokine Storm Signaling Pathway 371
Multiple Sclerosis Signaling Pathway 222
IL-12 Signaling and Production in Macrophages 236
Neutrophil Extracellular Trap Signaling Pathway 399
IL-13 Signaling Pathway 116
IL-15 Production 123
Atherosclerosis Signaling 133
0.0 0.2 0.4 0.6 0.8 1.0 1.2 1.4 1.6 1.8 2.0 2.2 2.4 2.6 2.8 3.0 3.2 3.4 3.6
-log(B-H p-value)